ZIRCON GEOCHRONOLOGY OF TOROK AND NANUSHUK FORMATIONS SANDSTONES AT SLOPE MOUNTAIN AND A SEABEE FORMATION TEPHRA DEPOSIT AT NINULUK BLUFF, CENTRAL NORTH SLOPE, ALASKA

Trystan M. Herriott, James L. Crowley, David L. LePain, Marwan A. Wartes, Nina T. Harun, and Mark D. Schmitz

Raw Data File 2024-33

Oblique aerial view northward across the southeast face of Slope Mountain, northern Alaska. The contact between the Torok and Nanushuk Formations lies at the base of the thick, resistant sandstone interval that extends prominently across the lower part of the photograph. Slope Mountain's summit is at the left skyline, with a ~1-km-thick Nanushuk Formation section exposed at this well-known locality.

2024
STATE OF ALASKA
DEPARTMENT OF NATURAL RESOURCES
DIVISION OF GEOLOGICAL & GEOPHYSICAL SURVEYS

STATE OF ALASKA
Mike Dunleavy, Governor

DEPARTMENT OF NATURAL RESOURCES
John Boyle, Commissioner

DIVISION OF GEOLOGICAL & GEOPHYSICAL SURVEYS
Melanie Werdon, State Geologist & Director

Publications produced by the Division of Geological & Geophysical Surveys are available to download from the DGGS website (dggs.alaska.gov). Publications on hard-copy or digital media can be examined or purchased in the Fairbanks office:

Alaska Division of Geological & Geophysical Surveys (DGGS)
3354 College Road | Fairbanks, Alaska 99709-3707
Phone: 907.451.5010 | Fax 907.451.5050
dggspubs@alaska.gov | dggs.alaska.gov

DGGS publications are also available at:

Alaska State Library, Historical
Collections & Talking Book Center
395 Whittier Street
Juneau, Alaska 99801

Alaska Resource Library and
Information Services (ARLIS)
3150 C Street, Suite 100
Anchorage, Alaska 99503

Suggested citation:
Herriott, T.M., Crowley, J.L., LePain, D.L., Wartes, M.A., Harun, N.T., and Schmitz, M.D., 2024, Zircon geochronology of Torok and Nanushuk Formations sandstones at Slope Mountain and a Seabee Formation tephra deposit at Ninuluk Bluff, central North Slope, Alaska: Alaska Division of Geological & Geophysical Surveys Raw Data File 2024-33, 42 p. https://doi.org/10.14509/31152

ZIRCON GEOCHRONOLOGY OF TOROK AND NANUSHUK FORMATIONS SANDSTONES AT SLOPE MOUNTAIN AND A SEABEE FORMATION TEPHRA DEPOSIT AT NINULUK BLUFF, CENTRAL NORTH SLOPE, ALASKA

Trystan M. Herriott[1], James L. Crowley[2], David L. LePain[1], Marwan A. Wartes[1], Nina T. Harun[1], and Mark D. Schmitz[2]

INTRODUCTION

Resolving the ages of Alaska's stratigraphic units is foundational to understanding sedimentary basin evolution and hydrocarbon potential. Existing stratal age constraints in Alaska often remain tied to paleontologic assessments completed during mid-twentieth century geologic mapping campaigns led by the U.S. Geological Survey (for example, Detterman and others, 1963). Although many of these relative-age frameworks reflect extensive fossil collections, the provinciality and wide or ambiguous age ranges for some faunas and floras, especially at high latitudes, can present notable hurdles to further understanding of basin histories.

U–Pb geochronology of zircon is starting to refine, or redefine, the chronostratigraphic frameworks in Alaska basins (for example, Herriott and others, 2019a, 2019b; Gillis and others, 2022; Lease and others, 2022). There are, however, challenges in absolute-age radioisotopic geochronology that should also be considered and mitigated to avoid overinterpreting results and resolve the research questions posed. In 2018, several authors of this current report conducted a pilot study of Jurassic strata in the Cook Inlet forearc basin of southern Alaska that aimed to delineate and mitigate common challenges in applications of detrital zircon (DZ) geochronology for establishing maximum depositional ages (MDAs) (Herriott and others, 2019a). Following that work, we expanded these efforts to include Brookian megasequence strata in the Mesozoic–Cenozoic Colville foreland basin of northern Alaska. One key to our approach is tandem dating of zircon, with moderate-precision (for example, ±3.2% at 2σ [single-analysis analytical uncertainty]) screening by laser ablation-inductively coupled plasma mass spectrometry (LA-ICPMS; see, for example, Gehrels and others, 2008) that is then complemented by subsequent high-precision (for example, ±0.08% at 2σ [single-analysis analytical uncertainty]) chemical abrasion-isotope dilution-thermal ionization mass spectrometry (CA-ID-TIMS; Mattinson, 2005) analyses of the youngest zircon crystals identified by LA-ICPMS (see Schoene [2014] and Schaltegger and others [2015] for reviews of U–Pb zircon geochronology mass spectrometry). Collaboration with Boise State University's Isotope Geology Laboratory has made it possible for DGGS to lead high-precision, zircon-based chronostratigraphy projects in Alaska.

[1] Alaska Division of Geological & Geophysical Surveys, 3354 College Road, Fairbanks, Alaska 99709
[2] Department of Geosciences, Boise State University, 1910 University Drive, Boise, Idaho 83725

This data release presents LA-ICPMS and CA-ID-TIMS U–Pb data for five DZ samples collected from a well-known exposure at Slope Mountain (for example, Huffman, 1989; Willingham and Herriott, 2020; figs. 1 and 2), which is one of the few localities where the transition between mid-Cretaceous Torok and Nanushuk Formations is preserved in outcrop (for example, Harris and others, 2002; Mull and others, 2003; LePain and others, 2009, 2022; fig. 3). We also report new U–Pb tephra zircon data from basal Seabee Formation at Ninuluk Bluff (figs. 1, 3, and 4), a key—and similarly rare—site where the transition between Late Cretaceous Nanushuk strata and overlying Seabee crops out (Detterman and others, 1963; LePain and others, 2009; LePain and Kirkham, 2024). These tandem-dated samples were collected during summer field seasons in 2018 and 2019 as part of DGGS's North Slope and Brooks Range foothills basin analysis program. The new zircon geochronology results from Slope Mountain and Ninuluk Bluff are documented and permanently archived here, and a detailed chronostratigraphic assessment of these new data is being prepared. Digital data associated with this report can be found at https://doi.org/10.14509/31152.

Stratigraphy, Sample Localities, and Existing Age Constraints

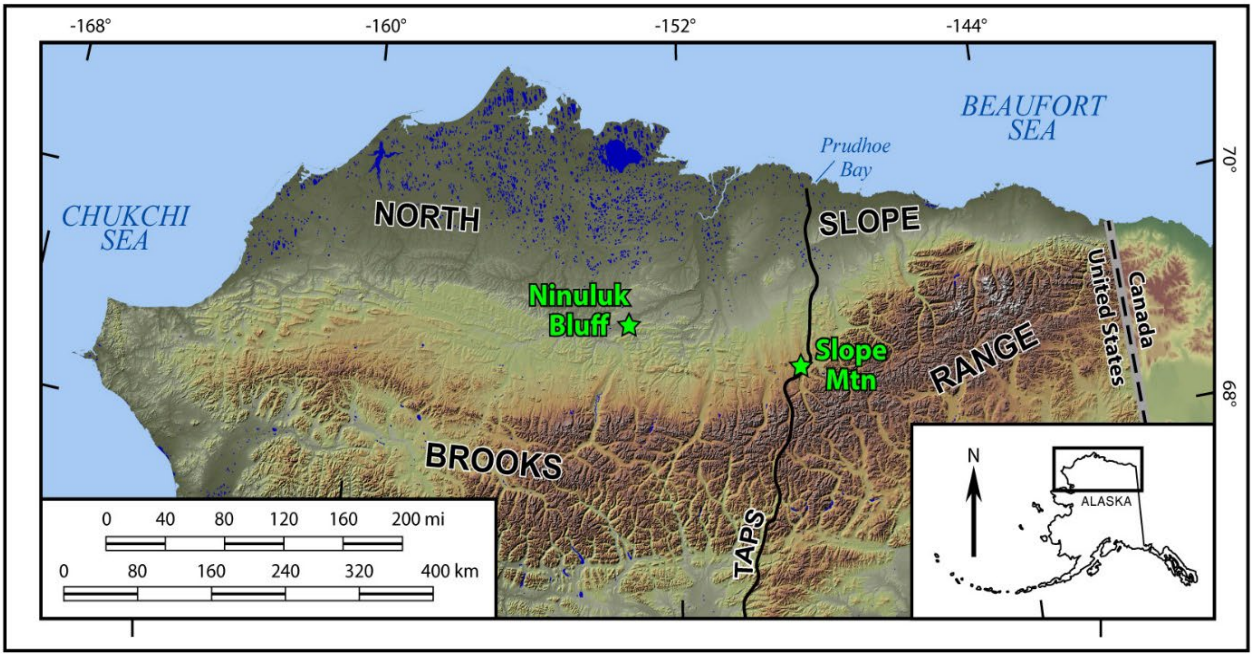

Figure 1. Northern Alaska location map, highlighting the Slope Mountain and Ninuluk Bluff localities of the east-central and west-central North Slope, respectively. See figures 2, 3, and 4 for sample site details. Abbreviations: Mtn—Mountain; TAPS: Trans-Alaska Pipeline System.

Regionally, Nanushuk Formation (non-marine and shallow-marine topset strata) and Torok Formation (deep-marine foreset [slope] and proximal bottomset [basin floor] strata) form a massive, up to 7,500-m-thick clinothem that records ~20 Ma of Aptian–Cenomanian Colville foreland basin sedimentation, with basal Seabee Formation strata marking basin-wide transgression and termination of principally regressive Nanushuk–Torok depositional systems (Houseknecht, 2019a; Lease and

others, 2022; also Bird and Andrews, 1979; Molenaar, 1983, 1985, 1988; Bird and Molenaar, 1992; Houseknecht and others, 2009; Bird and Houseknecht, 2011). Time-transgressive development of the clinothem is generally well understood, with growth mainly accomplished by northeastward to eastward progradation associated with continental-scale, basin-axial sediment routing systems (for example, Houseknecht 2019a; fig. 6 therein). The timing of this progradation was further delineated by the LA-ICPMS-based DZ MDA chronostratigraphic framework of Lease and others (2022).

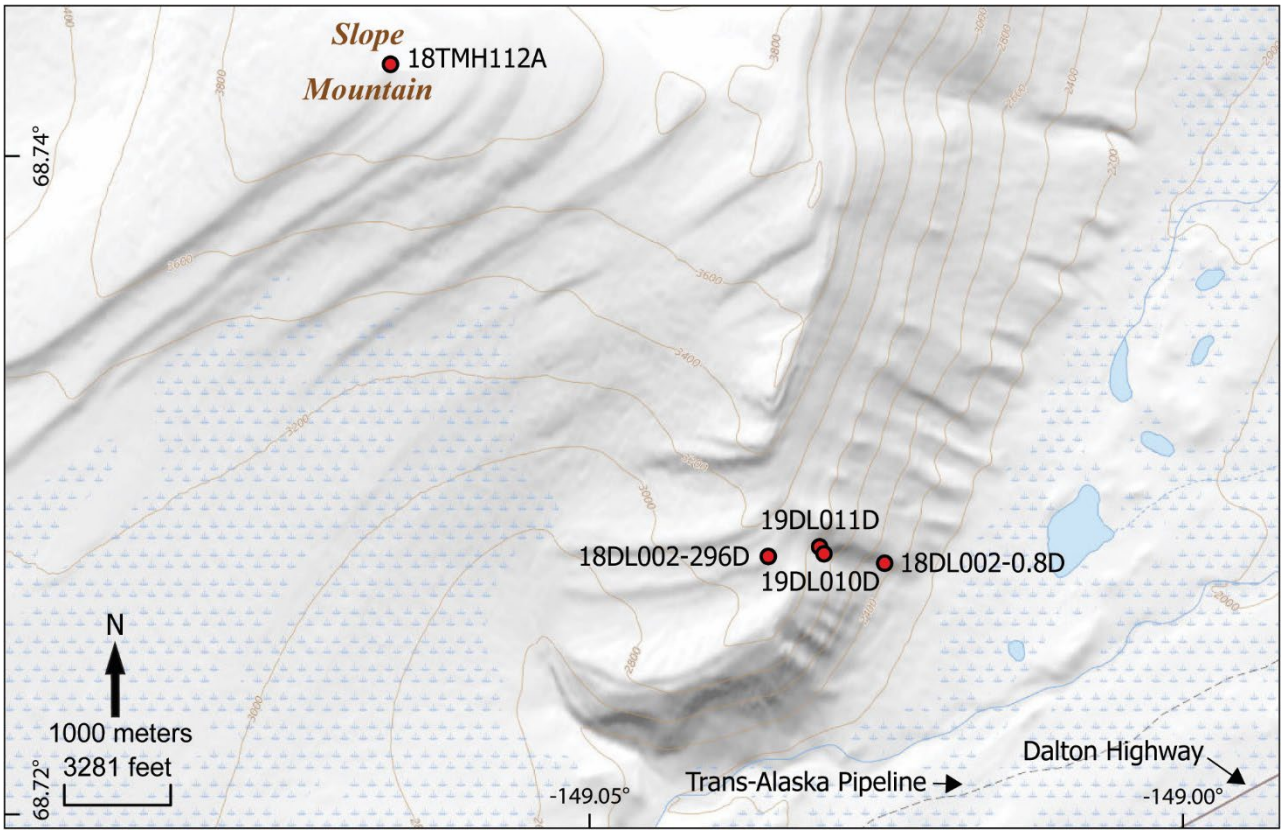

Figure 2. Slope Mountain locality map, showing the sample sites for detrital zircon results presented in this report.

LePain and others (2022) recently highlighted that sandstone-rich parasequences in the lower Nanushuk Formation at Slope Mountain can serve as outcrop analogues for Nanushuk reservoirs of recent major oil discoveries to the northwest. Refer to Houseknecht (2019b) for additional regional geologic context of the Colville foreland basin and to Houseknecht (2019a) for stratigraphic relations and petroleum geology of the Nanushuk–Torok stratigraphy (see also LePain and others, 2009; Helmold and LePain, 2023).

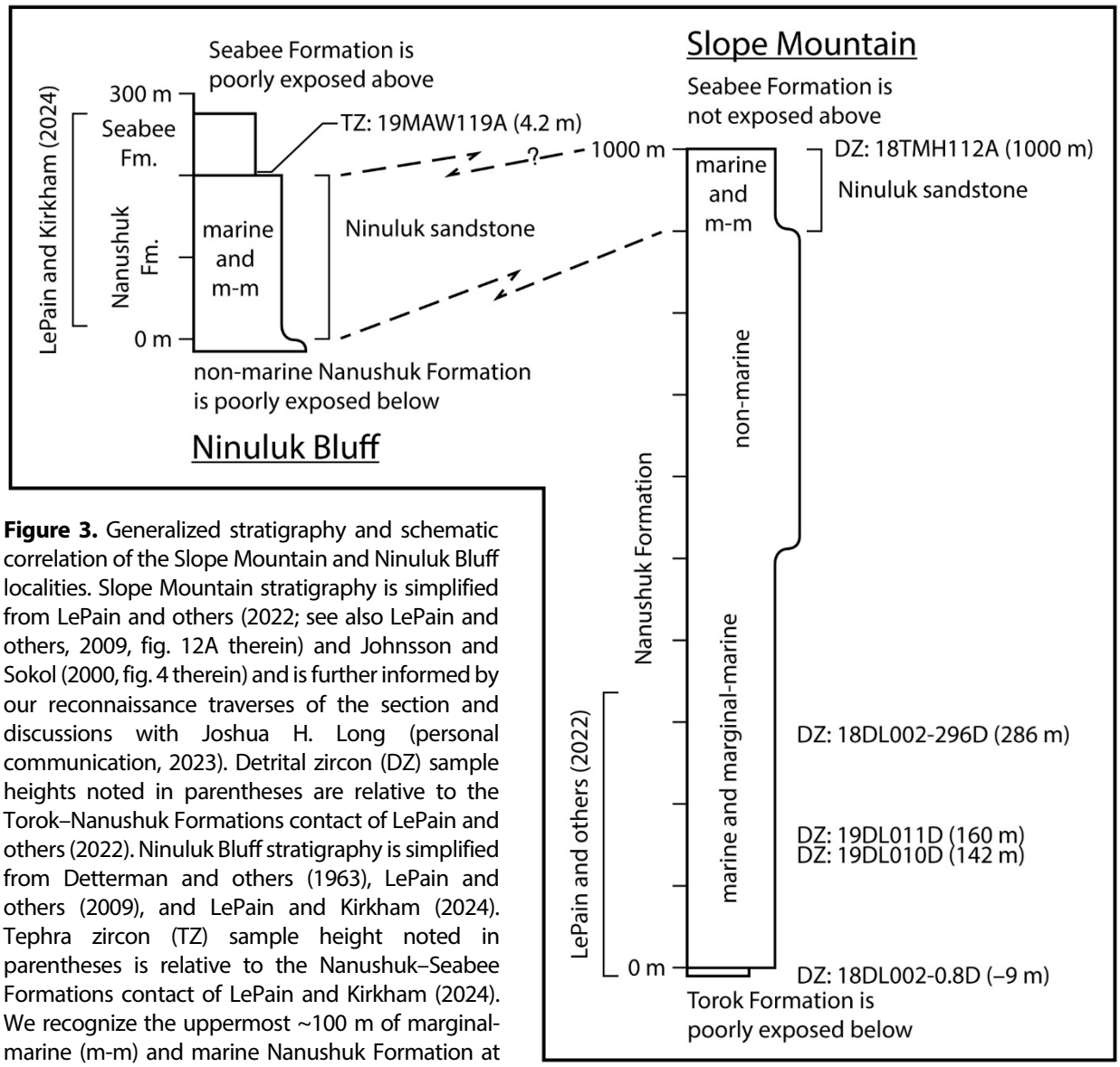

Figure 3. Generalized stratigraphy and schematic correlation of the Slope Mountain and Ninuluk Bluff localities. Slope Mountain stratigraphy is simplified from LePain and others (2022; see also LePain and others, 2009, fig. 12A therein) and Johnsson and Sokol (2000, fig. 4 therein) and is further informed by our reconnaissance traverses of the section and discussions with Joshua H. Long (personal communication, 2023). Detrital zircon (DZ) sample heights noted in parentheses are relative to the Torok–Nanushuk Formations contact of LePain and others (2022). Ninuluk Bluff stratigraphy is simplified from Detterman and others (1963), LePain and others (2009), and LePain and Kirkham (2024). Tephra zircon (TZ) sample height noted in parentheses is relative to the Nanushuk–Seabee Formations contact of LePain and Kirkham (2024). We recognize the uppermost ~100 m of marginal-marine (m-m) and marine Nanushuk Formation at Slope Mountain as the Ninuluk sandstone (see also Keller and others, 1961; LePain and others, 2009). The19MAW119A tephra zircon sample result of Ninuluk Bluff is correlated to the top of the Slope Mountain stratigraphy as a minimum age constraint. Note that uppermost Torok strata are interpreted as outer-shelf to upper-slope deposits; all Nanushuk and Seabee units depicted here are topset deposits, with lower Seabee at Ninuluk Bluff principally reflecting offshore sedimentation (LePain and others, 2009). Additional abbreviation: Fm.—Formation.

Slope Mountain: Torok and Nanushuk Formations

Slope Mountain lies in the Brooks Range foothills north of the mountain front on the east-central North Slope (figs. 1 and 2) and has been studied for many decades (for example, Keller and others, 1961; Huffman and others, 1981; Huffman, 1985; Johnsson and Sokol, 2000; LePain and others, 2009, 2022). This locality is relatively accessible along the Dalton Highway corridor near milepost 301 (for example, Huffman, 1989; Schenk and Bird, 1993; Harris and others, 2002; LePain

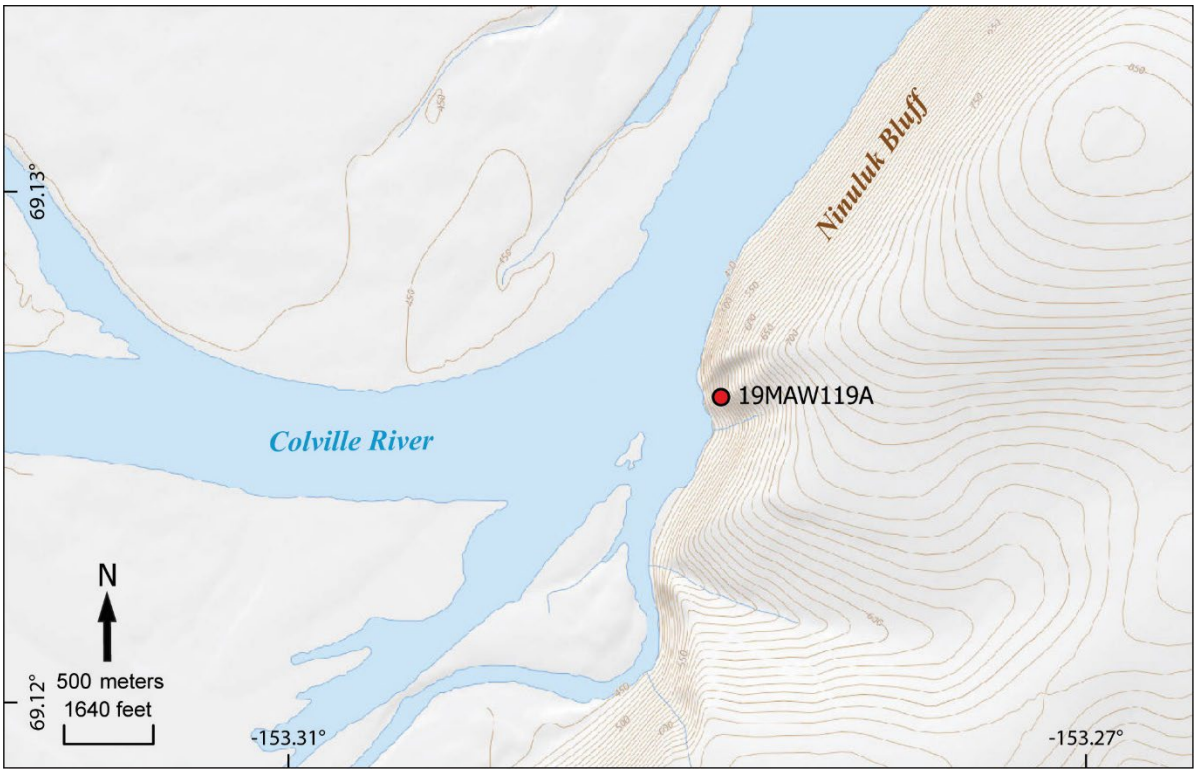

Figure 4. Ninuluk Bluff locality map, showing the sample site for tephra zircon results presented in this report.

and others, 2009, 2022). Uppermost Torok Formation of outer-shelf to upper-slope affinity occurs near the base of the exposure at Slope Mountain (LePain and others, 2022) and is overlain by a ~1000-m-thick Nanushuk Formation section comprising a shallow-marine and marginal-marine lower part, a non-marine middle part, and a marginal-marine and shallow-marine upper part (LePain and others, 2009 [discussion and fig. 12A therein]; also Keller and others, 1961; Huffman and others, 1981; Huffman, 1989; Johnsson and Sokol, 2000; this study; fig. 3).

Sedimentologic and stratigraphic details and interpretations for the uppermost 10 m of Torok Formation and lower 336.5 m of shallow-marine and marginal-marine Nanushuk Formation at Slope Mountain were provided by LePain and others (2022), with four of the five DZ sample results reported here tied to their measured section (figs. 2 and 3). The fifth Slope Mountain DZ sample (18TMH112A) of this report is from the top of the exposed stratigraphy immediately below the summit (figs. 2 and 3), where we observed marine trace fossils, including *Schaubcylindrichnus* and probable *Planolites*, *Thalassinoides*, and *Skolithos*, in Nanushuk strata. Additionally, indications of compensationally stacked bar forms associated with the 18TMH112A sample site suggest mouth bar sedimentation at a delta front (Peter P. Flaig, personal communication, 2022). We also observed *Schaubcylindrichnus* and probable *Planolites* within a recessive interval ~100 meters stratigraphically below the Slope Mountain summit, confirming the presence of a relatively thick—albeit thinner as preserved at Slope Mountain than at Ninuluk Bluff—marginal-marine and marine capping succession (fig. 3). Ultimately, we concur with the assessment of Keller and others (1961) that the upper part of Nanushuk Formation at Slope

Mountain regionally corresponds to the (former) Ninuluk formation (Detterman and others, 1963; Ninuluk sandstone herein; see below).

Ninuluk Bluff: Nanushuk and Seabee Formations

Ninuluk Bluff lies along the Colville River on the west-central North Slope (figs. 1 and 4) and has also been studied for many decades (for example, Detterman and others, 1963; Huffman and others, 1981; LePain and others, 2009; LePain and Kirkham, 2024). This bluff is the type locality for the (former) Ninuluk formation (Detterman and others, 1963; Mull and others (2003), a shallow-marine stratigraphic unit of uppermost Nanushuk Formation (Mull and others, 2003) that is now commonly referred to as the Ninuluk sandstone (for example, Houseknecht and Schenk, 2005; Lease and others, 2022; fig. 3). The Ninuluk sandstone is recognized as the record of retrogradational depositional systems leading up to transgressive cessation of Nanushuk–Torok sedimentation (for example, Houseknecht and Schenk, 2005; LePain and others, 2009; Lease and others, 2022; LePain and Kirkham, 2024). As noted above, the Nanushuk–Seabee Formations contact is exposed at Ninuluk Bluff, with lower Seabee strata interpreted as offshore deposits (LePain and others, 2009). LePain and Kirkham (2024) provide additional sedimentologic and stratigraphic details for Nanushuk and Seabee strata at this important locality.

Existing Age Constraints: Torok, Nanushuk, and Seabee Formations (central North Slope)

LePain and others (2009) reviewed biostratigraphic constraints for Nanushuk Formation of the central North Slope region, highlighting that ammonite and pelecypod fossils from lower Nanushuk strata along the outcrop trend between Slope Mountain and Ninuluk Bluff (fig. 1; see also LePain and others, 2009) are apparently as old as earliest middle Albian (~110 Ma; see Gale and others, 2020). LePain and others (2009) also presented marine microfossil constraints, with the lower, marine part of Nanushuk Formation at Slope Mountain yielding indications of middle and late Albian sedimentation. Farther up section at Slope Mountain, Keller and others (1961) noted an unfossiliferous stratigraphy and inferred that the middle, non-marine part of Nanushuk Formation at this locality is probably middle or late Albian and that the upper, marine succession is probably late Cenomanian based on regional correlations with the Ninuluk Bluff section (see also Detterman and other, 1963; fig. 3). The Seabee Formation, which regionally overlies the Nanushuk and Torok Formations, bears Turonian ammonites, pelecypods, and microfossils (for example, Mull and others, 2003) and has also yielded K–Ar and Ar/Ar dates that are often equivocal but suggestive of early Cenomanian to early Turonian sedimentation (Lanphere and Tailleur, 1983; Mull and others, 2003; Shimer and others, 2016). The Cenomanian–Turonian boundary is currently constrained at 93.9 Ma (Cohen and others, 2013; Gale and others, 2020).

More recently, Lease and others (2022) established DZ MDAs for more than a dozen Nanushuk–Torok paleo-shelf margins, with Nanushuk strata in the far west (Chukchi Sea area) being ~≤115 Ma and numerous indications that the end of Nanushuk–Torok clinothem sedimentation occurred at ~≤95 Ma. This Nanushuk–Torok Formations chronostratigraphic framework is tied to the

basin-axial, generally eastward advancing paleo-shelf margins of the clinothem north of the latitude of Ninuluk Bluff (Lease and others, 2022). To the south and east of Ninuluk Bluff, however, it is difficult to extrapolate in detail the framework of Lease and others (2022) to constrain, for example, the age of the Torok–Nanushuk Formations transition at Slope Mountain, due to several complicating factors, including: 1) the highly time-transgressive nature of Nanushuk and Torok Formations; 2) eastern deflection of the basin-axial, mainly north-south trending shelf-margins within the southern part of the Nanushuk–Torok clinothem (for example, Houseknecht, 2019a); and 3) increased fold-and-thrust-belt deformation and general scarcity of seismic reflection data in areas farther south (for example, Slope Mountain). Nevertheless, potentially synchronous cessation of Nanushuk–Torok depositional systems at ~≤95 Ma, as interpreted by Lease and others (2022), suggests widespread onset of Seabee Formation deposition during late Cenomanian time. Thus, published age constraints effectively bracket the Nanushuk Formation at Slope Mountain, and generally across the central North Slope (fig. 1), between ~110 Ma and ~94 Ma.

SAMPLES AND METHODS

Detrital zircon samples were collected from marine sandstone beds of the Torok and Nanushuk Formations, using typical field sampling protocols and taking great care to avoid contamination. Four of the DZ samples of this study are from the lower 296 m of the LePain and others (2022) section, and one additional DZ sample (18TMH112A) is from Nanushuk Formation at the top of the Slope Mountain stratigraphy (fig. 3). The tephra zircon sample was collected from a volcanic air-fall deposit in Seabee Formation at Ninuluk Bluff (fig. 3), taking similar care to avoid contamination.

Sample Descriptions (descending stratigraphic order)

19MAW119A: Seabee Formation (Ninuluk Bluff; tephra zircon)

Orange to yellow to white weathering, clayey, friable tephra deposit that ranges from 8 to 12 cm thick and includes black laminae of mudstone and lighter gray silty mudstone (siliciclastic components were not sampled). LePain and others (2009) interpreted the sampled Seabee succession as the record of offshore sedimentation (fig. 10C therein). The sample was collected from 4.2 meters above the Nanushuk–Seabee Formations contact (LePain and Kirkham, 2024; fig. 3); sample location coordinates are 69.12639°N 153.28822°W (WGS84).

18TMH112A: Nanushuk Formation (Slope Mountain; detrital zircon)

Fine-grained, very thin-bedded, cross-stratified, locally bioturbated sandstone; sampled package likely records delta front sedimentation (see above). The sample was collected from the top of the uppermost resistant sandstone package at Slope Mountain and is inferred to be 1000 m (rounded to the nearest 5 m) above the Torok–Nanushuk Formations contact of LePain and others (2022; fig. 3) based largely on the lithologic column of Johnsson and Sokol (2000, fig. 4 therein; see also Huffman and others, 1981; Schenk and Bird, 1993; LePain and others, 2009, 2022). The upper part of the Slope

Mountain stratigraphy is regionally correlated to the marine Ninuluk sandstone (see above). Sample location coordinates are 68.74270°N 149.06694°W (WGS84). Two sample bags were collected during 2018 and analyzed separately by LA-ICPMS in 2019 and 2021 in an effort to improve youthful zircon yields.

18DL002-296D: Nanushuk Formation (Slope Mountain; detrital zircon)

Medium-grained, thickly bedded, trough cross-stratified sandstone; sample is from the uppermost part of a resistant interval that LePain and others (2022) interpreted as a distributary channel fill package (see 290.0–296.2 m of sheet 1 and figs. 12B and 13B therein). The sample was collected from meter 296 of the measured section of LePain and others (2022), which is 286 m above the Torok–Nanushuk Formations contact of that study (fig. 3). Sample location coordinates are 68.72777°N 149.03506°W (WGS84).

19DL011D: Nanushuk Formation (Slope Mountain; detrital zircon)

Very fine-grained, thin- to medium-bedded sandstone, with moderate to high bioturbation index (LePain and others, 2022); the sampled sandstone package is interpreted to record lower shoreface or delta front(?) sedimentation (LePain and others, 2022; sheet 1 and fig. 11B therein). The sample was collected from meter 170.0 of the measured section of LePain and others (2022), which is 160 m above the Torok–Nanushuk Formations contact of that study (fig. 3). Sample location coordinates are 68.72806°N 149.03070°W (WGS84).

19DL010D: Nanushuk Formation (Slope Mountain; detrital zircon)

Very fine-grained, plane-parallel laminated sandstone; the sampled sandstone package exhibits convolute bedding and is interpreted to record delta front sedimentation (LePain and others, 2022; sheet 1 and fig. 9B therein). The sample was collected from meter 151.7 of the measured section of LePain and others (2022), which is 141.7 m above the Torok–Nanushuk Formations contact of that study (we assign a stratigraphic height of 142 m; fig. 3). Sample location coordinates are 68.72785°N 149.03033°W (WGS84).

18DL002-0.8D: Torok Formation (Slope Mountain; detrital zircon)

Very fine-grained, plane-parallel laminated sandstone; the sample is from the base of a sandstone interval that is ~80 cm thick, hosts *Phycosiphon* or *Helminthopsis* burrows in its upper portion, and likely records prodelta sedimentation in an outer-shelf to upper-slope setting that was subject to hyperpycnal flows (LePain and others, 2022; sheet 1 and fig. 5 therein). The sample was collected from meter 0.8 of the measured section of LePain and others (2022), which is 9.2 m below the Torok–Nanushuk Formations contact of that study (we assign a stratigraphic height of -9 m; fig. 3). Sample location coordinates are 68.72756°N 149.02518°W (WGS84).

U–Pb Zircon Geochronology: Methods Overview

Zircon from the Slope Mountain DZ samples and the Ninuluk Bluff tephra zircon sample were separated and analyzed by U–Pb geochronology at the Boise State University Isotope Geology Laboratory. All samples were analyzed first by LA-ICPMS, delineating the overall character of date distributions for the DZ samples and distinguishing approximately syn-eruptive versus clearly xenocrystic or otherwise older zircon for the tephra sample. The DZ samples were principally analyzed to establish MDAs, with LA-ICPMS serving as a moderate-precision screening tool to target youthful, near-stratal-age zircon for high-precision follow-up analysis by CA-ID-TIMS. All mid-Cretaceous DZ identified by LA-ICPMS were plucked from their epoxy mounts and analyzed by CA-ID-TIMS; in several cases, "a" and "b" zircon fragments from the same crystal were analyzed by CA-ID-TIMS to further evaluate reproducibly and accuracy of the results (see Herriott and others [2019a] for additional discussion of these protocols). A sub-set (n=6) of tephra zircon from the Ninuluk Bluff sample that yielded mid-Cretaceous LA-ICPMS dates were plucked for analyses by CA-ID-TIMS. Appendix A (included below) provides detailed analytical methods for the LA-ICPMS and CA-ID-TIMS experiments. Appendix B (included below) presents cathodoluminescence images of zircon analyzed during this study, including annotations with LA-ICPMS analysis numbers, laser ablation spot locations, z-grain (CA-ID-TIMS) designations, and dates and analytical uncertainties (2σ) for the CA-ID-TIMS results.

RESULTS

Mid-Cretaceous DZ dates are rare in the LA-ICPMS results for the Slope Mountain sandstones (n=0–2 per sample), whereas the Ninuluk Bluff tephra zircon sample yielded mostly mid-Cretaceous LA-ICPMS dates (n=11 of 14) (data file 1). As noted above, tandem dating by CA-ID-TIMS solely focused on zircon with mid-Cretaceous LA-ICPMS dates; complete CA-ID-TIMS results are in data file 2. Table 1 briefly summarizes the CA-ID-TIMS results, including MDAs for the Slope Mountain DZ samples and a depositional age for the Ninuluk Bluff tephra zircon sample; data file 3 also summarizes these results in a geodatabase-ready format. Data file 4 contains machine-readable summaries of the U–Pb zircon data (LA-ICPMS and CA-ID-TIMS). Data files 1–4 are available at doi.org/10.14509/31152.

CLOSING COMMENT

A chronostratigraphic analysis of the new CA-ID-TIMS-based age constraints from Slope Mountain and Ninuluk Bluff is in preparation; that treatment will also address considerations for establishing accurate and valid DZ MDAs in light of LA-ICPMS–CA-ID-TIMS tandem-date relations. This data release is part of DGGS's continued efforts to bring chronostratigraphic research in Alaska basins into higher resolution focus, with an emphasis on both precision and accuracy. Relatively few radioisotopic age constraints for Brookian strata have been published (for example, Shimer and others, 2016; LePain and others, 2021; Lease and others, 2022), and the record of Colville foreland basin depositional systems is remarkably extensive in time and space (Houseknecht, 2019b), providing many opportunities to conduct relevant, impactful studies. Additional CA-ID-TIMS zircon age constraints for Alaska's energy-resource-bearing sedimentary successions will be published pending completion of further analytical work and stratigraphic syntheses.

Table 1 (following page). Summary of U–Pb chemical abrasion-thermal ionization mass spectrometry (CA-ID-TIMS) results and interpreted ages from the Ninuluk Bluff tephra zircon (19MAW119A) and Slope Mountain detrital zircon (all others) samples. The dates are $^{206}Pb/^{238}U$ results. Interpreted ages reflect weighted means of multiple tephra zircon dates for 19MAW119A and multiple fragment dates from a single detrital zircon for 18TMH112A, 18DL002-296D, and 18DL002-0.8D; note that the 19DL010D maximum depositional age (MDA) is based on a single analysis and 19DL011D did not yield mid-Cretaceous laser ablation-inductively coupled mass spectrometry (LA-ICPMS) dates. Individual z-grain date uncertainties only include analytical (also known as internal or random) sources; uncertainties for interpreted ages (depositional age [DA] for tephra zircon; MDA for detrital zircon) are reported as X (Y) [Z], reflecting analytical, (analytical with tracer), and [analytical with tracer and decay constant] sources (see appendix A). Stratigraphic position, or height, for all DZ samples is relative to the base of Nanushuk Formation at Slope Mountain (see text) and as meters above top of Nanushuk Formation for the Ninuluk Bluff tephra zircon sample. Complete LA-ICPMS and CA-ID-TIMS results are in data files 1 and 2, respectively. MSWD = mean square weighted deviation; PoF = probability of fit.

Table 1.

Sample	Formation	Stratigraphic position (m)	CA-ID-TIMS										
			Date (Ma)	± 2σ (Ma)	Analysis ID	Include in age?	DA (Ma)	MDA (Ma)	± 2σ (Ma)	n (zircon)	n (dates)	MSWD	PoF
19MAW119A	Seabee	+4.2	94.866	0.078	z1 (XXS 428)	x	**94.909**	--	**0.032 (0.042) [0.110]**	6	6	1.10	0.36
			94.889	0.071	z2 (XXS 429)	x							
			94.947	0.078	z3 (XXS 434)	x							
			94.886	0.071	z4 (XXS 437)	x							
			94.985	0.095	z5 (XXS 441)	x							
			94.914	0.079	z6 (XXS 428)	x							
18TMH112A	Nanushuk	1000	102.40	0.04	z1a (M 132)	x	--	**102.41**	**0.03 (0.06) [0.13]**	1	2	2.68	0.10
			102.48	0.08	z1b (M 132	x							
18DL002-296D	Nanushuk	286	100.90	0.08	z1a (M 272)	x	--	**100.88**	**0.08 (0.09) [0.14]**	1	2	0.94	0.33
			100.78	0.22	z1b (M 272)	x							
19DL011D	Nanushuk	160	--	--	--	--	--	--	--	--	--	--	--
19DL010D	Nanushuk	142	101.19	0.08	z1 (XS 461)	x	--	**101.19**	**0.08 (0.09) [0.14]**	1	1	--	--
18DL002-0.8D	Torok	–9	101.58	0.13	z1a (S 138)	x	--	**101.58**	**0.13 (0.14) [0.18]**	1	2	1.08	0.30
			100.85	1.41	z1b (S 138)	x							

ACKNOWLEDGMENTS

Our base camp for several recent field seasons was at Toolik Field Station, which is placed on and surrounded by "the ancestral hunting grounds of the Nunamiut, and occasional hunting grounds and routes of the Gwich'in, Koyukuk, and Iñupiaq peoples" (www.uaf.edu/toolik/about/land-acknowledgement.php); these surrounding lands include Slope Mountain and some of the earliest known Alaska Native peoples sites in northern Alaska. We thank Arctic Slope Regional Corporation for granting access to their lands at Ninuluk Bluff, with Erik Kenning processing our permit requests.

Our chronostratigraphic work in northern Alaska has benefited from discussions with Richard Lease, Peter Flaig, Joshua Long, Robert Gillis, Jared Gooley, David Houseknecht, Amanda Willingham, and Mareca Guthrie. Amanda Willingham and Michelle Gavel participated in our Slope Mountain fieldwork during 2018. Robin Carbaugh digitized laser ablation spot locations and labels on the cathodoluminescence imagery of appendix B and joined us on several traverses at Slope Mountain and Ninuluk Bluff. We thank the staff and managers of Toolik Field Station and Happy Valley for hosting our field crews. Tom "Rat" Ratledge and Sarah Rafaelli safely transported personnel during fieldwork. Kristen Janssen and Simone Montayne provided publication support. Reviews by Robert Gillis and an anonymous referee improved this data report.

The State of Alaska funded this study, and funding for the analytical infrastructure of the Boise State University Isotope Geology Laboratory is provided by the National Science Foundation (grants EAR-0521221, EAR-0824974, EAR-1337887, EAR-1735889).

REFERENCES

Bird, K.J., and Andrews, J., 1979, Subsurface studies of the Nanushuk Group, North Slope, Alaska, *in* Ahlbrandt, T.S., ed., Preliminary geologic, petrologic, and paleontologic results of the study of Nanushuk Group rocks, North Slope, Alaska: U.S. Geological Survey Circular 794, p. 32–41. https://doi.org/10.3133/cir794

Bird, K.J., and Houseknecht, D.W., 2011, Geology and petroleum potential of the Arctic Alaska petroleum province, *in* Spencer, A.M., Embry, A.F., Gautier, D.L., Stoupakova, A.V., and Sørensen, Kai, eds., Arctic petroleum geology: Memoirs of the Geological Society of London, v. 35, ch. 32, p. 485–499. https://doi.org/10.1144/M35.32

Bird, K.J., and Molenaar C.M., 1992, The North Slope foreland basin, *in* Macqueen, R.W., and Leckie, D.A., eds., Foreland basins and foldbelts: American Association of Petroleum Geologists Memoir 55, p. 363–393. https://doi.org/10.1306/M55563C14

Cohen, K.M., Finney, S.C., Gibbard, P.L. and Fan, J.-X., (2013; updated v. 2023/09: https://stratigraphy.org/chart [accessed 25 October 2023]), The ICS International Chronostratigraphic Chart: Episodes, v. 36, p. 199–204. https://doi.org/10.18814/epiiugs/2013/v36i3/002

Detterman, R.L., Bickel, R.S., and Gryc, George, 1963, Geology of the Chandler River region, Alaska: U.S. Geological Survey Professional Paper 303-E, p. 233–324, 16 sheets, scale 1:125,000. https://doi.org/10.3133/pp303E

Gale, A.S., Mutterlose, J., Batenburg, S., Gradstein, F.M., Agterberg, F.P., Ogg, J.G., Petrizzo, M.R., 2020, The Cretaceous Period, *in* Gradstein, F.M., Ogg, J.G., Schmitz, M.D., and Ogg, G.M., eds., Geologic Time Scale 2020: Elsevier, v.2, ch. 27, p. 1023–1086, https://doi.org/10.1016/B978-0-12-824360-2.00027-9

Gehrels, G.E., Valencia, V.A., and Ruiz, J., 2008, Enhanced precision, accuracy, efficiency, and spatial resolution of U–Pb ages by laser ablation–multicollector–inductively coupled plasma–mass spectrometry: Geochemistry, Geophysics, Geosystems, v. 9, Q03017, 13 p. https://doi.org/10.1029/2007GC001805

Gillis, R.J., Wartes, M.A., Herriott, T.M., LePain, D.L., Benowitz, J.A., Wypych, Alicja, Donelick, R.A., O'Sullivan, P.B., and Layer, P.W., 2022, $^{40}Ar/^{39}Ar$ and U–Pb geochronology of Cretaceous–Paleocene igneous rocks and Cenozoic strata of northwestern Cook Inlet, Alaska: Linkages between arc magmatism, cooling, faulting, and forearc subsidence: Alaska Division of Geological & Geophysical Surveys Professional Report 125, v. 1.1, 78 p. https://doi.org/10.14509/30554

Harris, E.E., Mull, C.G., Reifenstuhl, R.R., and Montayne, Simone, 2002, Geologic map of the Dalton Highway (Atigun Gorge to Slope Mountain) area, southern Arctic Foothills, Alaska: Alaska Division of Geological & Geophysical Surveys Preliminary Interpretive Report 2002-2, 1 sheet, scale 1:63,360. https://doi.org/10.14509/2867

Helmold, K.P., and LePain, D.L., 2023, Controls on reservoir quality of the Nanushuk Formation (Albian–Cenomanian), North Slope, Alaska: Marine and Petroleum Geology, v. 148, 105877. https://doi.org/10.1016/j.marpetgeo.2022.105877

Herriott, T.M., Crowley, J.L., Schmitz, M.D., Wartes, M.A., and Gillis, R.J., 2019a, Exploring the law of detrital zircon: LA-ICP-MS and CA-TIMS geochronology of Jurassic forearc strata, Cook Inlet, Alaska, USA: Geology, v. 47, p. 1044–1048. https://doi.org/10.1130/G46312.1

Herriott, T.M., Wartes, M.A., O'Sullivan, P.B., and Gillis, R.J., 2019b, Detrital zircon maximum depositional dates for the Jurassic Chinitna and Naknek Formations, lower Cook Inlet, Alaska: A preliminary view: Alaska Division of Geological & Geophysical Surveys Preliminary Interpretive Report 2019-5, 11 p. https://doi.org/10.14509/30180

Houseknecht, D.W., 2019a, Petroleum systems framework of significant new oil discoveries in a giant Cretaceous (Aptian–Cenomanian) clinothem in Arctic Alaska: American Association of Petroleum Geologists Bulletin, v. 103, p. 619–652, https://doi.org/10.1306/08151817281

Houseknecht, D.W., 2019b, Evolution of the Arctic Alaska sedimentary basin, *in* Miall, A.D., ed., The Sedimentary Basins of the United States and Canada, 2nd edition: Elsevier, ch. 18, p. 719–745. https://doi.org/10.1016/B978-0-444-63895-3.00018-8

Houseknecht, D.W., Bird, K.J., and Schenk, C.J., 2009, Seismic analysis of clinoform depositional sequences and shelf-margin trajectories in Lower Cretaceous (Albian) strata, Alaska North Slope: Basin Research, v. 21, p. 644–654. https://doi.org/10.1111/j.1365-2117.2008.00392.x

Houseknecht, D.W., and Schenk, C.J., 2005, Sedimentology and sequence stratigraphy of the Cretaceous Nanushuk, Seabee, and Tuluvak Formations exposed on Umiat Mountain, north-central Alaska, *in* Haeussler, P.J., and Galloway, J.P., eds., Studies by the U.S. Geological Survey in Alaska, 2004: U.S. Geological Survey Professional Paper 1709-B, 18 p. https://doi.org/10.3133/pp1709B

Huffman, A.C., Ahlbrandt, T.S., Pasternack, Ira, Stricker, G.D., Bartsch-Winkler, Susan, Fox, J.E., May, F.E., and Scott, R.A., 1981, Measured sections in the Cretaceous Nanushuk and Colville groups undivided, central North Slope, Alaska: U.S. Geological Survey Open-File Report 81-177, 162 p. https://doi.org/10.3133/ofr81177

Huffman, A.C., Jr., ed., 1985, Geology of the Nanushuk Group and related rocks, North Slope, Alaska: U.S. Geological Survey Bulletin 1614, 129 p. https://doi.org/10.3133/b1614

Huffman, A.C., Jr., 1989, The Nanushuk Group, *in* Mull, C.G., and Adams, K.E., eds., Bedrock geology of the eastern Koyukuk basin, central Brooks Range, and east-central Arctic Slope along the Dalton Highway, Yukon River to Prudhoe Bay, Alaska, Volume 2: Alaska Division of Geological & Geophysical Surveys Guidebook 7-21, p. 303–309. https://doi.org/10.14509/24135

Johnsson, M.J., and Sokol, N.K., 2000, Stratigraphic variation in petrographic composition of Nanushuk Group sandstones at Slope Mountain, North Slope, Alaska, *in* Kelley, K.D., and Gough, L.P., eds., Geologic studies in Alaska by the U. S. Geological Survey, 1998: U.S. Geological Survey Professional Paper 1615, p. 83–100. https://doi.org/10.3133/70180644

Keller, A.S., Morris, R.H., and Detterman, R.L., 1961, Geology of the Shaviovik and Sagavanirktok rivers region, Alaska: U.S. Geological Survey Professional Paper 303-D, p. 169–222, 6 sheets. https://doi.org/10.3133/pp303D

Lanphere, M.A., and Tailleur, I.L., 1983, K–Ar ages of bentonites in the Seabee Formation, northern Alaska: A Late Cretaceous (Turonian) time-scale point: Cretaceous Research, v. 4, p. 361–370. https://doi.org/10.1016/S0195-6671(83)80004-4

Lease, R.O., Houseknecht, D.W., and Kylander-Clark, A.R.C., 2022, Quantifying large-scale continental shelf margin growth and dynamics across middle-Cretaceous Arctic Alaska with detrital zircon U–Pb dating: Geology, v. 50, p. 620–625. https://doi.org/10.1130/G49118.1

LePain, D.L., Harun, N.T., and Kirkham, R.A., 2022, Measured stratigraphic section, lower Nanushuk Formation (Albian), Slope Mountain (Marmot syncline), Alaska: Alaska Division of Geological & Geophysical Surveys Preliminary Interpretive Report 2022-1, 21 p., 1 sheet. https://doi.org/10.14509/30871

LePain, D.L., McCarthy, P.J., and Kirkham, R.A., 2009, Sedimentology and sequence stratigraphy of the middle Albian–Cenomanian Nanushuk Formation in outcrop, central North Slope, Alaska: Alaska Division of Geological & Geophysical Surveys Report of Investigation 2009-1, v. 2, 76 p., 1 sheet. https://doi.org/10.14509/19761

LePain, D.L., and Kirkham, R.A., 2024, Measured stratigraphic section, upper Nanushuk Formation (Cenomanian), Ninuluk Bluff, Alaska: Alaska Division of Geological & Geophysical Surveys Preliminary Interpretive Report 2024-3, 28 p., 1 sheet. https://doi.org/10.14509/31150

LePain, D.L., Wartes, M.A., Kirkham, R.A., and Mongrain, J.R., 2021, Measured stratigraphic section in the upper Schrader Bluff Formation (Late Campanian–Maastrichtian?), Ivishak River, Alaska: Alaska Division of Geological & Geophysical Surveys Preliminary Interpretive Report 2021-3, 11 p., 1 sheet. https://doi.org/10.14509/30693

Mattinson, J.M., 2005, Zircon U–Pb chemical abrasion ("CA-TIMS") method: Combined annealing and multi-step partial dissolution analysis for improved precision and accuracy of zircon ages: Chemical Geology, v. 220, p. 47–66. https://doi.org/10.1016/j.chemgeo.2005.03.011

Molenaar, C.M., 1983, Depositional relations of Cretaceous and lower Tertiary rocks, northeastern Alaska: American Association of Petroleum Geologists Bulletin, v. 67, p. 1,066–1,080. https://doi.org/10.1306/03B5B6FF-16D1-11D7-8645000102C1865D

Molenaar, C.M., 1985, Subsurface correlations and depositional history of the Nanushuk Group and related strata, North Slope, Alaska, *in* Huffman, A.C., ed., Geology of the Nanushuk Group and related rocks, North Slope, Alaska: U.S. Geological Survey Bulletin 1614, p. 37–59. https://doi.org/10.3133/b1614

Molenaar, C.M.,1988, Depositional history and seismic stratigraphy of Lower Cretaceous rocks in the National Petroleum Reserve in Alaska and adjacent areas, *in* Gryc, George, ed., Geology and exploration of the National Petroleum Reserve in Alaska, 1974 to 1982: U.S. Geological Survey Professional Paper 1399, p. 593–621. https://doi.org/10.3133/pp1399

Mull, C.G., Houseknecht, D.W., and Bird, K.J., 2003, Revised Cretaceous and Tertiary Stratigraphic Nomenclature in the Colville basin, northern Alaska: U.S. Geological Survey Professional Paper 1673, 59 p. https://doi.org/10.3133/pp1673

Schaltegger, U., Schmitt, A.K., and Horstwood, M.S.A., 2015, U–Th–Pb zircon geochronology by ID-TIMS, SIMS, and laser ablation ICP-MS: Recipes, interpretations, and opportunities: Chemical Geology, v. 402, p. 89–110. https://doi.org/10.1016/j.chemgeo.2015.02.028

Schenk, C.J., and Bird, K.J., 1993, Depositional sequences in Lower Cretaceous rocks, Atigun Syncline and Slope Mountain areas, Alaskan North Slope, *in* Dusel-Bacon, C., and Till, A.B., eds., Geologic studies in Alaska by the U.S. Geological Survey, 1992: U.S. Geological Survey Bulletin 2068, p. 48–58. https://doi.org/10.3133/b2068

Schoene, B., 2014, U–Th–Pb geochronology, *in* Rudnick, R.L., ed., Treatise on Geochemistry (second edition), Volume 4: The Crust: Elsevier, ch. 4.10, p. 341–378. https://doi.org/10.1016/B978-0-08-095975-7.00310-7

Shimer, G.T., Benowitz, J.A., Layer, P.W., McCarthy, P.J., Hanks, C.L., and Wartes, Marwan, 2016, $^{40}Ar/^{39}Ar$ ages and geochemical characterization of Cretaceous bentonites in the Nanushuk, Seabee, Tuluvak, and Schrader Bluff formations, North Slope, Alaska: Cretaceous Research, v. 57, p. 325–341. https://doi.org/10.1016/j.cretres.2015.04.008

Willingham, A.L., and Herriott, T.M., 2020, Photogrammetry-derived digital surface model and orthoimagery of Slope Mountain, North Slope, Alaska, June 2018: Alaska Division of Geological & Geophysical Surveys Raw Data File 2020-1, 9 p. https://doi.org/10.14509/30419

APPENDICES

Appendix A. U–Pb zircon geochronology methods for laser ablation-inductively coupled plasma mass spectrometry and chemical abrasion-isotope dilution-thermal ionization mass spectrometry (included below).

Appendix B. Cathodoluminescence images of zircon analyzed during this study (included below). Laser ablation spot locations, analysis labels, and all mid-Cretaceous laser ablation-inductively coupled plasma mass spectrometry dates and analytical uncertainties (2σ) are included as annotations (black and white labels). Chemical abrasion-isotope dilution-thermal ionization mass spectrometry dates and analytical uncertainties (2σ) are noted for the tandem-dated crystals (see orange z-grain labels).

DATA FILES

Data File 1. Laser ablation-inductively coupled plasma mass spectrometry U–Pb geochronology and related data (six .xls files are available for download here: https://doi.org/10.14509/31152). Each Excel file includes instrumental data, sample data, standard data, and data dictionary worksheets. A. Seabee Formation, Ninuluk Bluff, tephra zircon, sample 19MAW119A. B. Nanushuk Formation, Slope Mountain, detrital zircon, sample 18TMH112A. C. Nanushuk Formation, Slope Mountain, detrital zircon, sample 18DL002-296D. D. Nanushuk Formation, Slope Mountain, detrital zircon, sample 19DL011D. E. Nanushuk Formation, Slope Mountain, detrital zircon, sample 19DL010D. F. Torok Formation, Slope Mountain, detrital zircon, sample 18DL002-0.8D.

Data File 2. Chemical abrasion-isotope dilution-thermal ionization mass spectrometry U–Pb zircon geochronology data (one .xls file is available for download here: https://doi.org/10.14509/31152) for tephra zircon sample (Ninuluk Bluff) 19MAW119A and detrital zircon samples (Slope Mountain) 18TMH112A, 18DL002-296D, 19DL010D, and 18DL002-0.8D. Slope Mountain detrital zircon sample 19DL011D did not yield Cretaceous $^{206}Pb/^{238}U$ dates by laser ablation-inductively coupled plasma mass spectrometry, and thus there are no isotope dilution data for that sample. A data dictionary worksheet is also included in the Excel file.

Data File 3. Summary of interpreted ages in a geodatabase-ready format (A), as well as a data dictionary (B) (two .csv files are available for download here: https://doi.org/10.14509/31152).

Data File 4. Summaries of the U–Pb zircon geochronology data in machine-readable formats. A. Laser ablation-inductively coupled plasma mass spectrometry data. B. Data dictionary for A. C. Chemical abrasion-isotope dilution-thermal ionization mass spectrometry data. D. Data dictionary for C. (four .csv files are available for download here: https://doi.org/10.14509/31152).

APPENDIX A. U–PB ZIRCON GEOCHRONOLOGY METHODS

Laser Ablation-Inductively Coupled Plasma Mass Spectrometry

Zircon grains were separated from rocks using standard techniques, annealed at 900°C for 60 hours in a muffle furnace, and mounted in epoxy and polished until their centers were exposed. Cathodoluminescence (CL) images (appendix B) were obtained with a JEOL JSM-300 scanning electron microscope and Gatan MiniCL. Zircon was analyzed by laser ablation-inductively coupled plasma mass spectrometry (LA-ICPMS) using two different platforms. Four samples (19MAW119A, 18TMH112A [bag 2], 19DL011D, 19DL010D) were analyzed during 2021 using an iCAP RQ Quadrupole ICP-MS and Teledyne Photon Machines Analyte Excite+ 193 nm excimer laser ablation system with HelEx II Active two-volume ablation cell. In-house analytical protocols, standard materials, and data reduction software were used for acquisition and calibration of U–Pb dates and a suite of high field strength elements and rare earth elements. Zircon was ablated with a laser spot of 20 µm wide using fluence and pulse rates of 2.5 J/cm^2 and 10 Hz, respectively, during a 25 second analysis (15 second gas blank, 10 second ablation) that excavated a pit ~8 µm deep. Ablated material was carried by a 0.25 L/min He gas stream in the inner cell and a 1.25 L/min He gas stream in the outer cell. Three samples (18TMH112A [bag 1], 18DL002-296D, 18DL002-0.8D) were analyzed during 2019 using a ThermoElectron X-Series II quadrupole ICPMS and New Wave Research UP-213 Nd:YAG UV (213 nm) laser ablation system. In-house analytical protocols, standard materials, and data reduction software were used for acquisition and calibration of U–Pb dates and a suite of high field strength elements and rare earth elements. Zircon was ablated with a laser spot of 25 µm wide using fluence and pulse rates of 5 J/cm^2 and 5 Hz, respectively, during a 45 second analysis (15 second gas blank, 30 second ablation) that excavated a pit ~15 µm deep. Ablated material was carried by a 1.2 L/min He gas stream to the nebulizer flow of the plasma. Dwell times and other instrumental data are given in the "Instrumental data" worksheet for each data file 1 (available at https://doi.org/10.14509/31152) Excel file. Background count rates for each analyte were obtained prior to each spot analysis and subtracted from the raw count rate for each analyte. Ablations pits that appear to have intersected glass or mineral inclusions were identified based on Ti and P. U–Pb dates from these analyses are considered valid if the U–Pb ratios appear to have been unaffected by the inclusions. Analyses that appear contaminated by common Pb were rejected based on mass 204 being above baseline. For concentration calculations, background-subtracted count rates for each analyte were internally normalized to ^{29}Si and calibrated with respect to NIST SRM-610 and -612 glasses as the primary standards. Temperature was calculated from the Ti-in-zircon thermometer (Watson and others, 2006). Because there are no constraints on the activity of TiO_2, an average value in crustal rocks of 0.6 was used.

The primary standard Plešovice zircon (Sláma and others, 2008) was used to monitor time-dependent instrumental fractionation based on two analyses for every 12 analyses of unknown zircon. A secondary correction to the ^{206}Pb/^{238}U dates was made based on results from the zircon standards Seiland (531 Ma, Kuiper and others, 2022), 91500 (1065 Ma, Wiedenbeck and others, 1995), and Zirconia (327 Ma, Boise State University, unpublished data) which were treated as unknowns and measured once for every 10–12 analyses of unknown zircon. These results (see "Standard data"

worksheet for each data file 1 Excel file) showed a linear age bias of several percent that is related to the ^{206}Pb count rate. The secondary correction is thought to mitigate matrix-dependent variations due to contrasting compositions and ablation characteristics between the Plešovice zircon and other standards (and unknowns).

Radiogenic isotope ratio and age error propagation for all analyses includes uncertainty contributions from counting statistics and background subtraction. Errors without and with the standard calibration uncertainty are shown in the "Sample data" worksheet for each data file 1 Excel file. This uncertainty is the local standard deviation of the polynomial fit to the interspersed primary standard measurements versus time for the time-dependent, relatively larger U/Pb fractionation factor, and the standard error of the mean of the consistently time-invariant and smaller $^{207}Pb/^{206}Pb$ fractionation factor. These uncertainties are given in the "Instrumental data" worksheet for each data file 1 Excel file. For groups of analyses that are collectively interpreted from a weighted mean date, a weighted mean date is first calculated from equivalent dates (probability of fit >0.05) using Isoplot 3.0 (Ludwig, 2003) with errors on individual dates that do not include a standard calibration uncertainty. A standard calibration uncertainty is then propagated into the error on the date. Discordance is calculated as the relative difference between $^{207}Pb/^{235}U$ and $^{206}Pb/^{238}U$ dates; unless otherwise noted on "Instrumental data" worksheet(s) for each data file 1 Excel file, analyses with discordance outside of uncertainty of 5% are formatted with strike-through and placed at the bottom of the "Sample data" worksheet for each data file 1 Excel file. Errors are at 2σ.

Chemical Abrasion-Isotope Dilution Thermal Ionization Mass Spectrometry

U–Pb dates were obtained by the chemical abrasion-isotope dilution-thermal ionization mass spectrometry (CA-ID-TIMS) method from analyses composed of single zircon grains or fragments of grains (data file 2; available at https://doi.org/10.14509/31152), modified after Mattinson (2005). Zircon was removed from the epoxy mounts for isotope dilution dating based on LA-ICPMS data (data file 1) and CL imagery (appendix B).

Zircon was put into 3 ml Teflon PFA beakers and loaded into 300 µl Teflon PFA microcapsules. Fifteen microcapsules were placed in a large-capacity Parr vessel and the zircon partially dissolved in 120 µl of 29 M HF for 12 hours at 190°C. Zircon was returned to 3 ml Teflon PFA beakers, HF was removed, and zircon was immersed in 3.5 M HNO_3, ultrasonically cleaned for an hour, and fluxed on a hotplate at 80°C for an hour. The HNO_3 was removed, and zircon was rinsed twice in ultrapure H_2O before being reloaded into the 300 µl Teflon PFA microcapsules (rinsed and fluxed in 6 M HCl during sonication and washing of the zircon) and spiked with the EARTHTIME mixed ^{233}U-^{235}U-^{202}Pb-^{205}Pb tracer solution (ET2535) or the EARTHTIME mixed ^{233}U-^{235}U-^{205}Pb tracer solution (ET535). Three samples were spiked with ET2535 and two samples were spiked with ET535 (data file 2). Zircon was dissolved in Parr vessels in 120 µl of 29 M HF with a trace of 3.5 M HNO_3 at 220°C for 48 hours, dried to fluorides, and re-dissolved in 6 M HCl at 180°C overnight. U and Pb were separated from the zircon matrix using an HCl-based anion-exchange chromatographic procedure (Krogh, 1973), eluted together and dried with 2 µl of 0.05 N H_3PO_4.

Pb and U were loaded on a single outgassed Re filament in 5 µl of a silica-gel/phosphoric acid mixture (Gerstenberger and Haase, 1997), and U and Pb isotopic measurements made on a GV Isoprobe-T multicollector thermal ionization mass spectrometer equipped with an ion-counting Daly detector. Pb isotopes were measured by peak-jumping all isotopes on the Daly detector for 160 cycles, and corrected for mass fractionation using the known $^{202}Pb/^{205}Pb$ ratio of the ET2535 tracer solution. Transitory isobaric interferences due to high-molecular weight organics, particularly on ^{204}Pb and ^{207}Pb, disappeared within approximately 30 cycles, while ionization efficiency averaged 10^4 cps/pg of each Pb isotope. Linearity (to $\geq 1.4 \times 10^6$ cps) and the associated deadtime correction of the Daly detector were determined by analysis of NBS982. U was analyzed as UO_2^+ ions in static Faraday mode on 10^{12} ohm resistors for 300 cycles, and corrected for isobaric interference of $^{233}U^{18}O^{16}O$ on $^{235}U^{16}O^{16}O$ with an $^{18}O/^{16}O$ of 0.00206. Ionization efficiency averaged 20 mV/ng of each U isotope. U mass fractionation was corrected using the known $^{233}U/^{235}U$ ratio of the ET2535 tracer solution.

U–Pb dates and uncertainties were calculated using the algorithms of Schmitz and Schoene (2007), calibration of ET2535 tracer solution (Condon and others, 2015) of $^{235}U/^{205}Pb$ = 100.233, $^{233}U/^{235}U$ = 0.99506, $^{205}Pb/^{204}Pb$ = 8474, and $^{202}Pb/^{205}Pb$ = 0.99924, calibration of ET535 tracer solution (Condon and others, 2015) of $^{235}U/^{205}Pb$ = 100.233, $^{233}U/^{235}U$ = 0.99506, and $^{205}Pb/^{204}Pb$ = 11268, U decay constants recommended by Jaffey and others (1971), and $^{238}U/^{235}U$ of 137.818 (Hiess and others, 2012). The $^{206}Pb/^{238}U$ ratios and dates were corrected for initial ^{230}Th disequilibrium using $D_{Th/U} = 0.2 \pm 0.1$ (2σ) and the algorithms of Crowley and others (2007), resulting in an increase in the $^{206}Pb/^{238}U$ dates of ~0.09 Ma. All common Pb in analyses was attributed to laboratory blank and subtracted based on the measured laboratory Pb isotopic composition and associated uncertainty. U blanks are estimated at 0.013 pg.

Weighted mean $^{206}Pb/^{238}U$ and $^{207}Pb/^{206}Pb$ dates are calculated from equivalent dates (probability of fit >0.05) using Isoplot 3.0 (Ludwig, 2003). Errors on weighted mean and single analysis $^{206}Pb/^{238}U$ interpreted ages are given as ± X (Y) [Z], where X is the internal error based on analytical uncertainties only, including counting statistics, subtraction of tracer solution, and blank and initial common Pb subtraction, Y includes the tracer calibration uncertainty propagated in quadrature, and Z includes the ^{238}U decay constant uncertainty propagated in quadrature. Internal errors should be considered when comparing our dates with $^{206}Pb/^{238}U$ dates from other laboratories that used the same tracer solution or a tracer solution that was cross-calibrated using EARTHTIME gravimetric standards. Errors including the uncertainty in the tracer calibration should be considered when comparing our dates with those derived from other geochronological methods using the U–Pb decay scheme (for example, LA-ICPMS). Errors including uncertainties in the tracer calibration and ^{238}U decay constant (Jaffey and others, 1971) should be considered when comparing our dates with those derived from other decay schemes (for example, $^{40}Ar/^{39}Ar$, ^{187}Re–^{187}Os). Errors are at 2σ.

References

Condon, D.J., Schoene, B., McLean, N.M., Bowring, S.A., and Parrish, R.R., 2015, Metrology and traceability of U–Pb isotope dilution geochronology (EARTHTIME Tracer Calibration Part I): Geochimica et Cosmochimica Acta, v. 164, p. 464–480, https://doi.org/10.1016/j.gca.2015.05.026

Crowley, J.L., Schoene, B., and Bowring, S.A., 2007, U–Pb dating of zircon in the Bishop Tuff at the millennial scale: Geology, v. 35, p. 1123–1126, https://doi.org/10.1130/G24017A.1.

Gerstenberger, H., and Haase, G., 1997, A highly effective emitter substance for mass spectrometric Pb isotope ratio determinations: Chemical Geology, v. 136, p. 309–312, https://doi.org/10.1016/S0009-2541(96)00033-2

Hiess, J., Condon, D.J., McLean, N., and Noble, S.R., 2012, $^{238}U/^{235}U$ systematics in terrestrial uranium-bearing minerals: Science, v. 335, p. 1610–1614, https://doi.org/10.1126/science.1215507

Jaffey, A.H., Flynn, K.F., Glendenin, L.E., Bentley, W.C., and Essling, A.M., 1971, Precision measurements of half-lives and specific activities of ^{235}U and ^{238}U: Physical Review C, v. 4, p. 1889–1906

Krogh, T.E., 1973, A low-contamination method for hydrothermal decomposition of zircon and extraction of U and Pb for isotopic age determination: Geochimica et Cosmochimica Acta, v. 37, p. 485–494, https://doi.org/10.1016/0016-7037(73)90213-5.

Kuiper, Y.D., Murray, D.P., Ellison, S., and Crowley, J.L., 2022, U–Pb detrital zircon analysis of sedimentary rocks of the southeastern New England Avalon terrane in the U.S. Appalachians: Evidence for a separate crustal block, *in* Kuiper, Y.D., Murphy, J.B., Nance, R.D., Strachan, R.A., and Thompson, M.D., eds., New Developments in the Appalachian-Caledonian-Variscan Orogen: Geological Society of America Special Paper 554, p. 93–119, https://doi.org/10.1130/2021.2554(05)

Ludwig, K.R., 2003, User's Manual for Isoplot 3.00: Berkeley Geochronology Center, Berkeley, California, 70 p.

Mattinson, J.M., 2005, Zircon U–Pb chemical abrasion ("CA-TIMS") method: Combined annealing and multi-step partial dissolution analysis for improved precision and accuracy of zircon ages: Chemical Geology, v. 220, p. 47–66, https://doi.org/10.1016/j.chemgeo.2005.03.011

Schmitz, M.D., and Schoene, B., 2007, Derivation of isotope ratios, errors, and error correlations for U–Pb geochronology using ^{205}Pb-^{235}U-(^{233}U)-spiked isotope dilution thermal ionization mass spectrometric data: Geochemistry, Geophysics, Geosystems, Q08006, https://doi.org/10.1029/2006GC001492

Sláma, J., Košler, J, Condon, D.J., Crowley, J.L., Gerdes, A., Hanchar, J.M., Horstwood, M.S.A., Morris, G.A., Nasdala, L., Norberg, N., Schaltegger, U., Schoene, B., Tubrett, M.N., and Whitehouse, M.J., 2008, Plešovice zircon—A new natural reference material for U–Pb and Hf isotopic microanalysis: Chemical Geology, v. 249, p. 1–35, https://doi.org/10.1016/j.chemgeo.2007.11.005

Watson, E.B., Wark, D.A., and Thomas, J.B., 2006, Crystallization thermometers for zircon and rutile: Contributions to Mineralogy and Petrology, v.151, p. 413–433, https://doi.org/10.1007/s00410-006-0068-5

Wiedenbeck, M., Allé, P., Corfu, F., Griffin, W.L., Meier, M., Oberli, F., von Quadt, A., Roddick, J.C., and Spiegel, W., 1995, Three natural zircon standards for U–Th–Pb, Lu–Hf, trace element and REE analyses: Geostandards Newsletter, v. 19, p. 1–23, https://doi.org/10.1111/j.1751-908X.1995.tb00147.x

APPENDIX B. CATHODOLUMINESCENCE IMAGES OF ZIRCON

19MAW119A XXS Seabee Formation tephra zircon AK DGGS BSU0630-0634 24Feb21

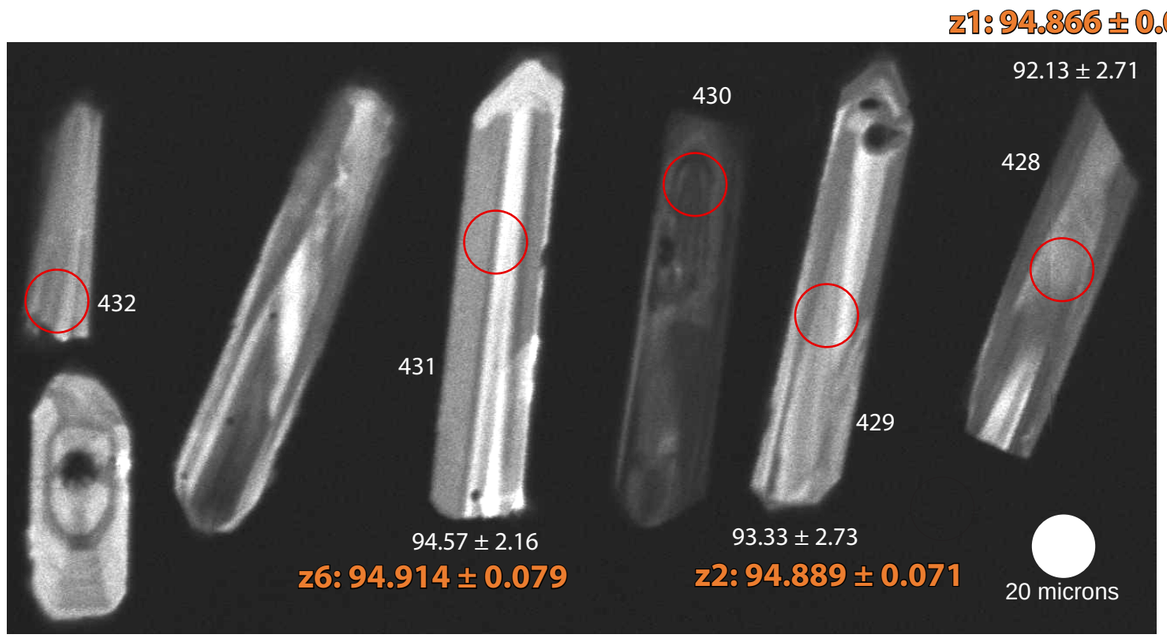

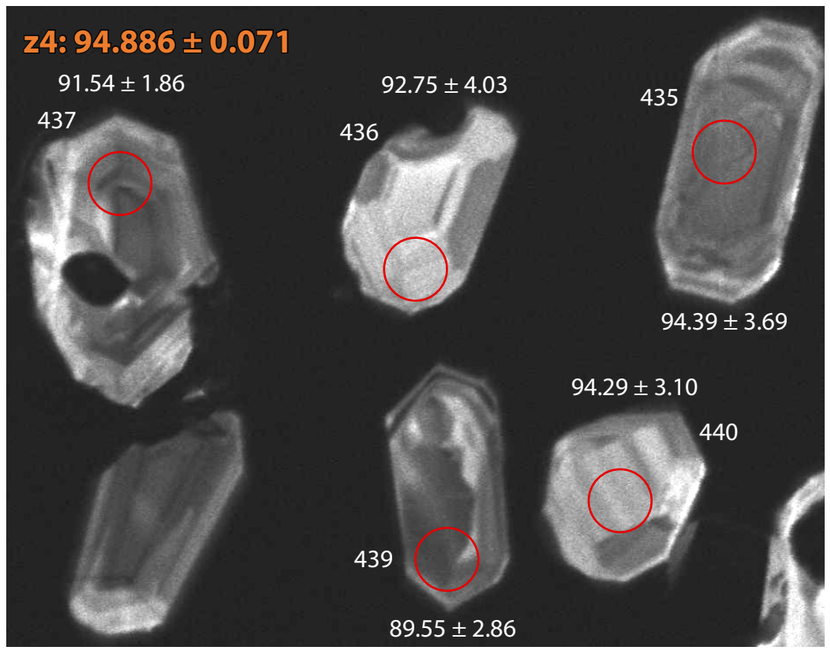

18TMH112A (2019) M row 1 & 2 Nanushuk Formation detrital zircon AK DGGS BSU0443-0446 20Sept19

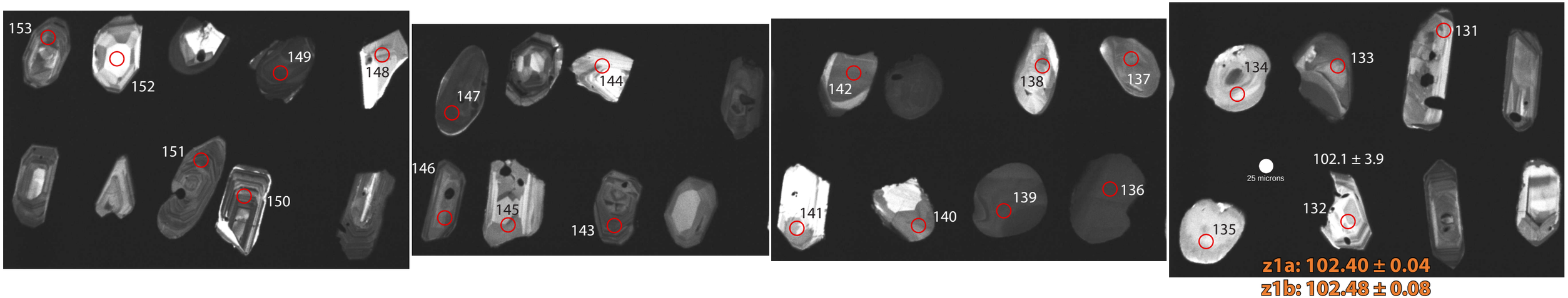

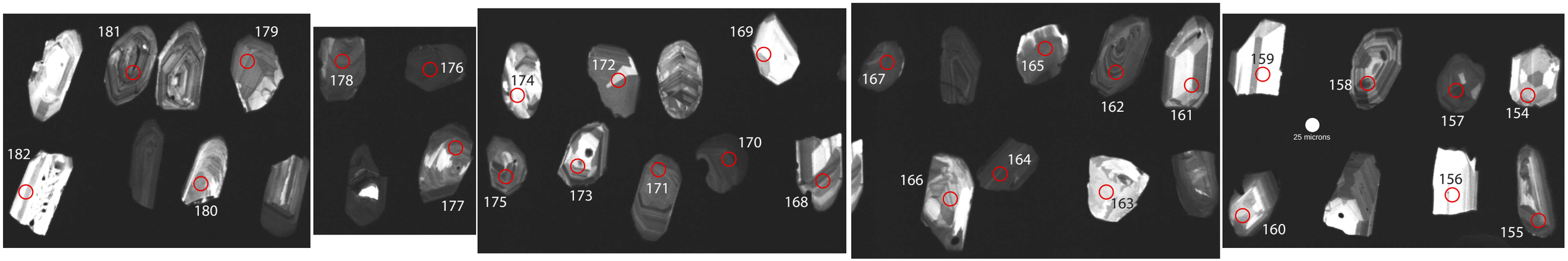

18TMH112A (2019) M row 3 Nanushuk Formation detrital zircon AK DGGS BSU0443-0446 20Sept19

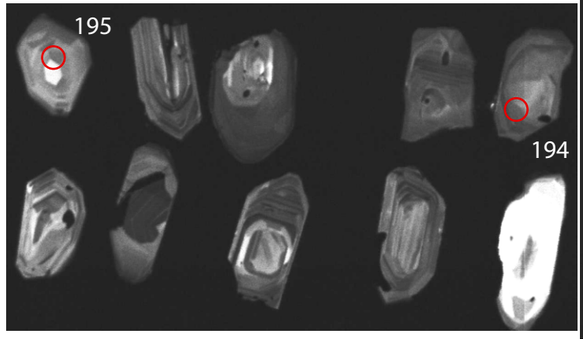

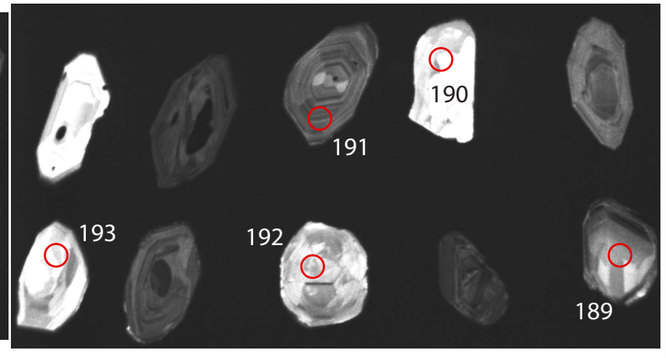

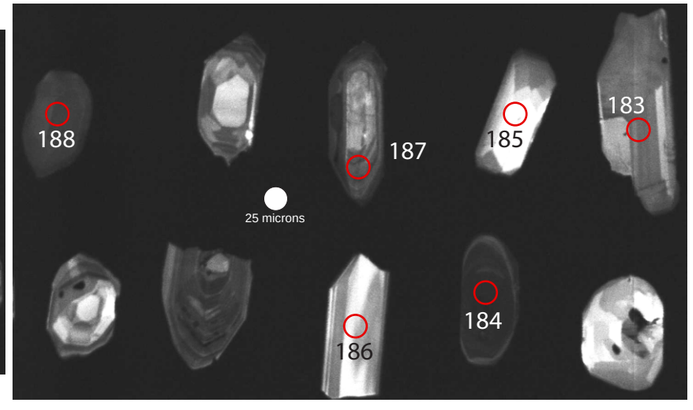

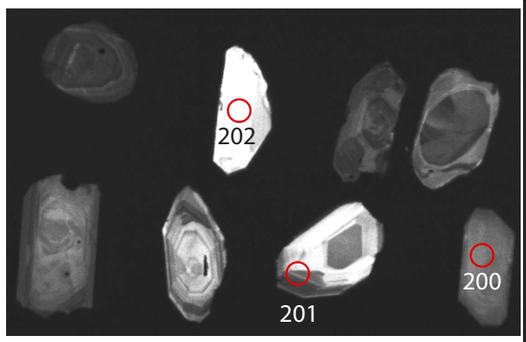

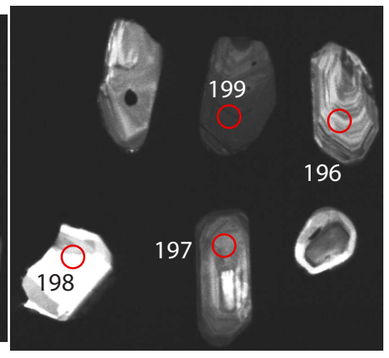

18TMH112A (2019) S row 1 Nanushuk Formation detrital zircon AK DGGS BSU0443-0446 20Sept19

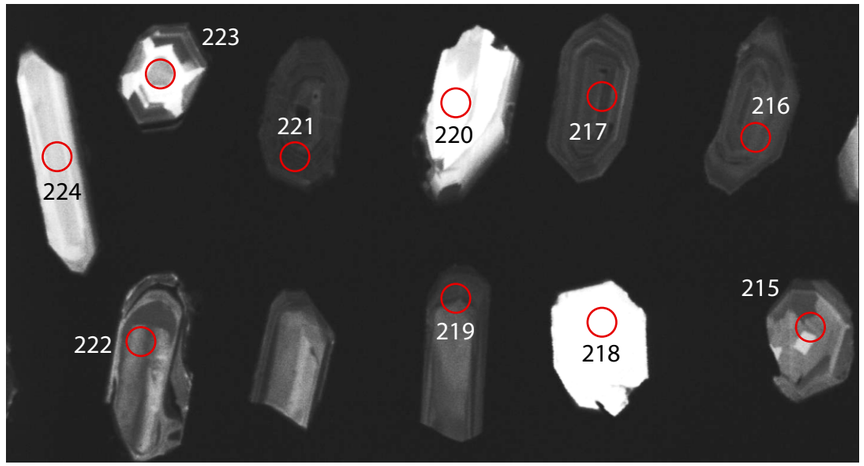

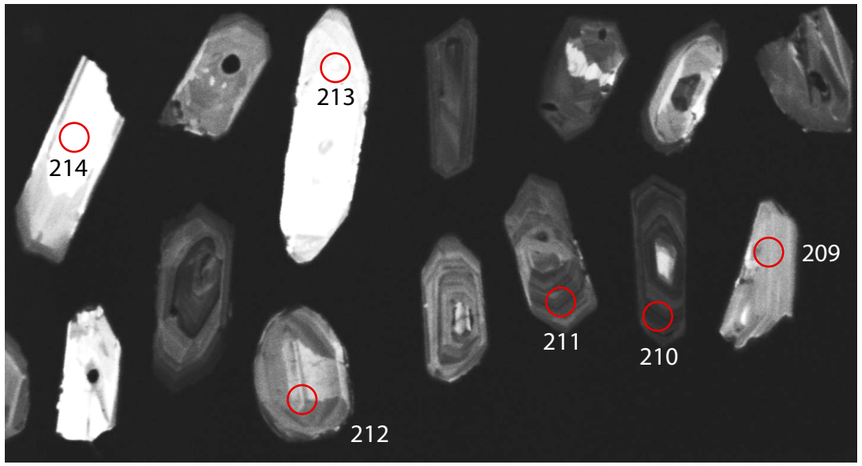

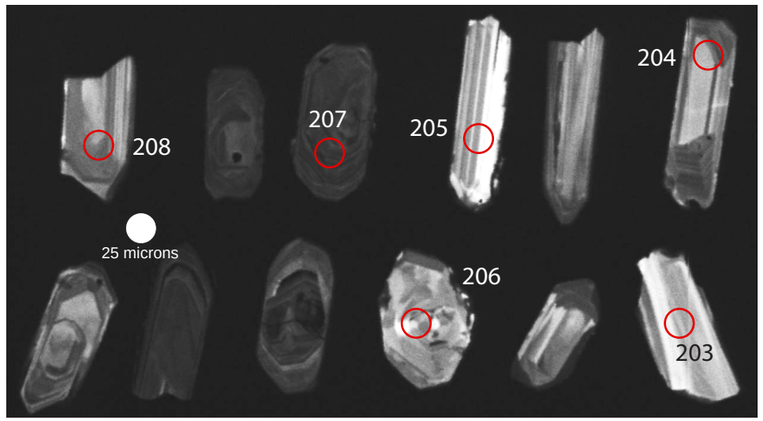

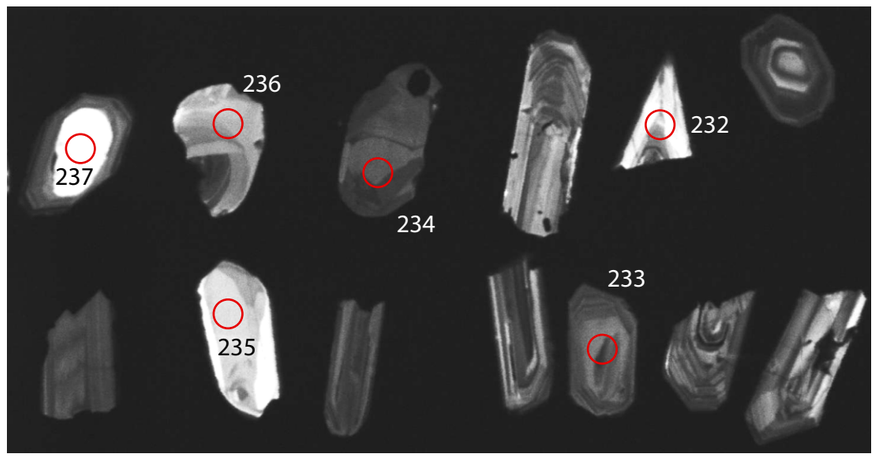

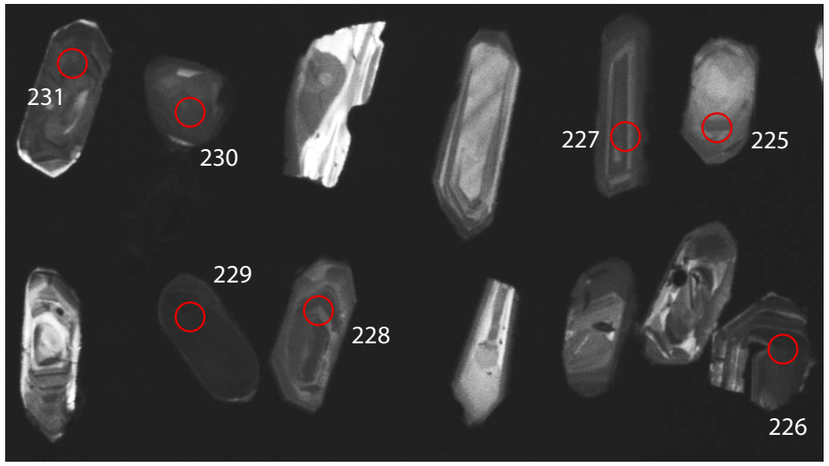

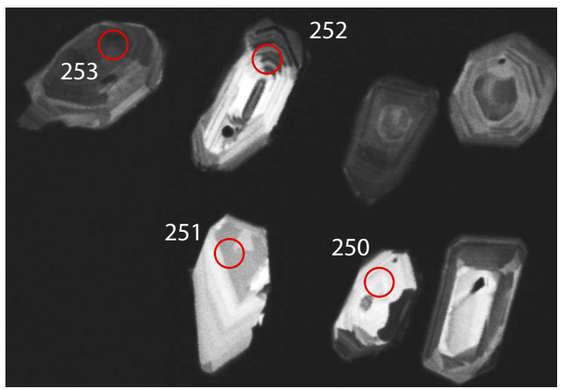

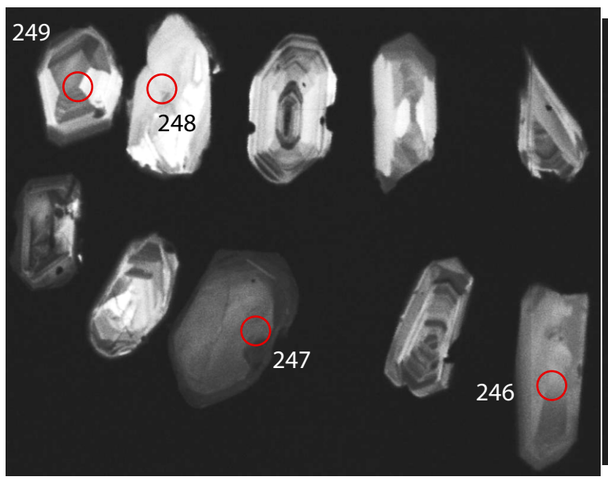

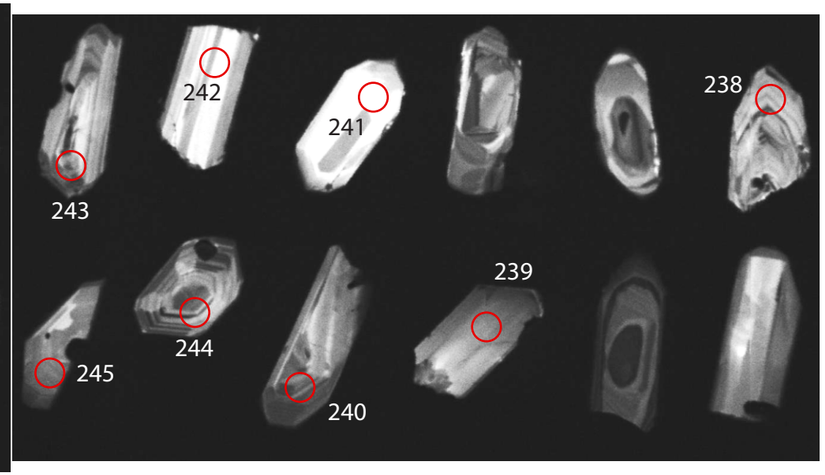

18TMH112A (2019) S row 2 Nanushuk Formation detrital zircon AK DGGS BSU0443-0446 20Sept19

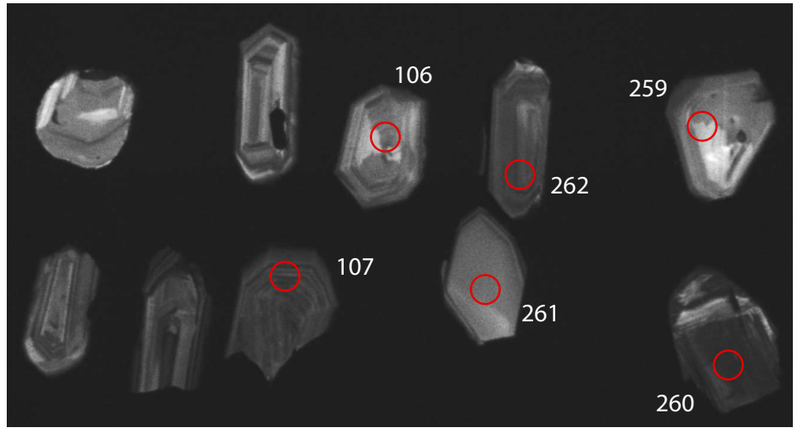

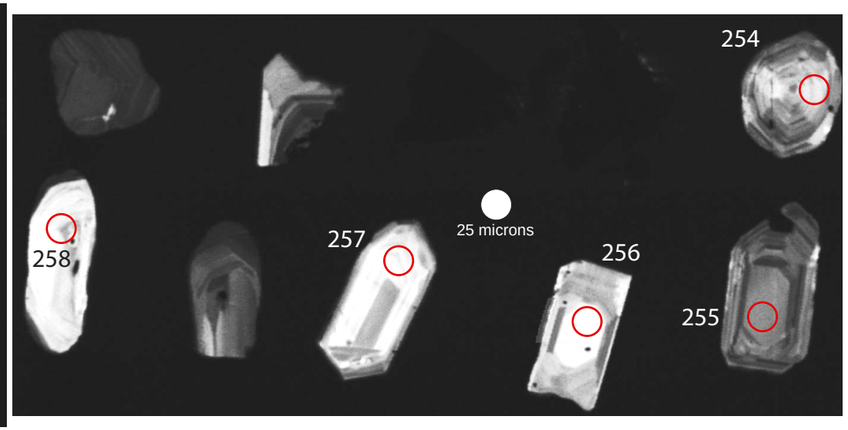

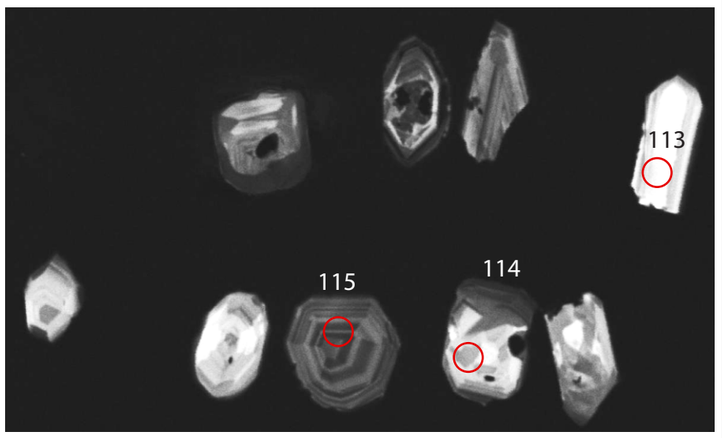

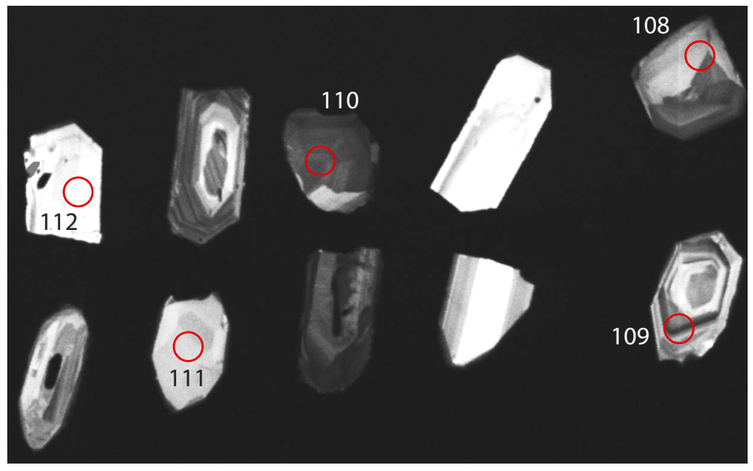

18TMH112A (2021) S Nanushuk Formation detrital zircon AK DGGS BSU0630-0634 24Feb21

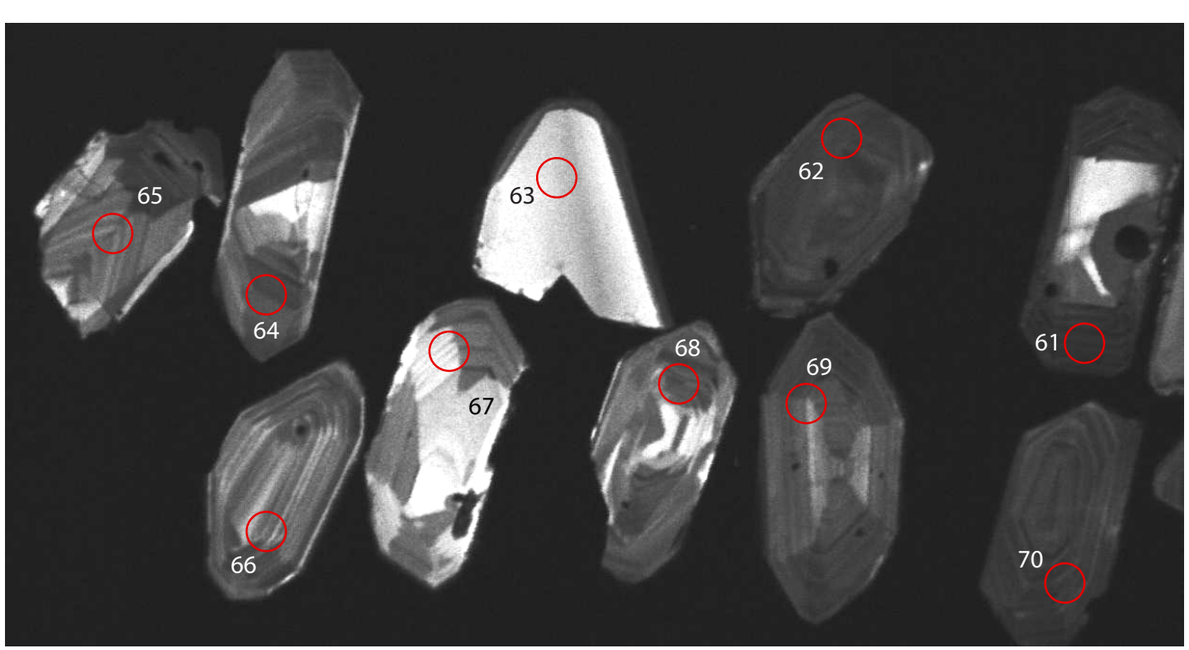

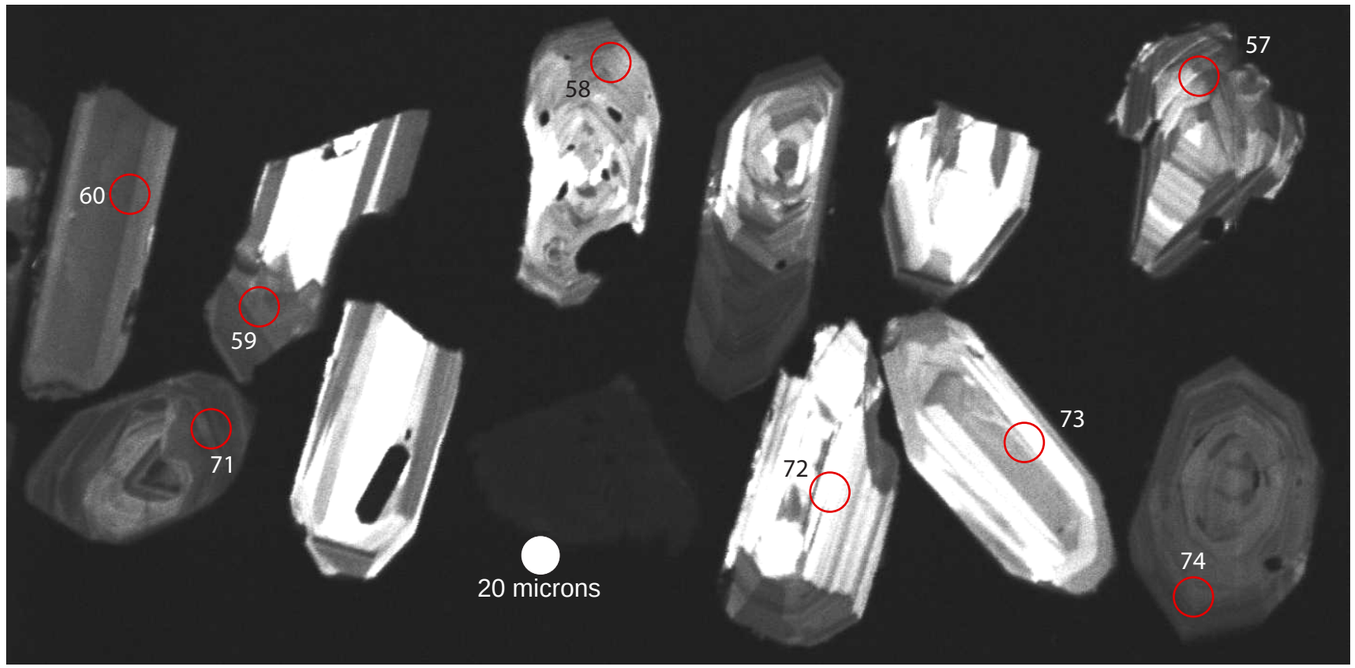

18TMH112A (2021) XS Nanushuk Formation detrital zircon AK DGGS BSU0630-0634 24Feb21

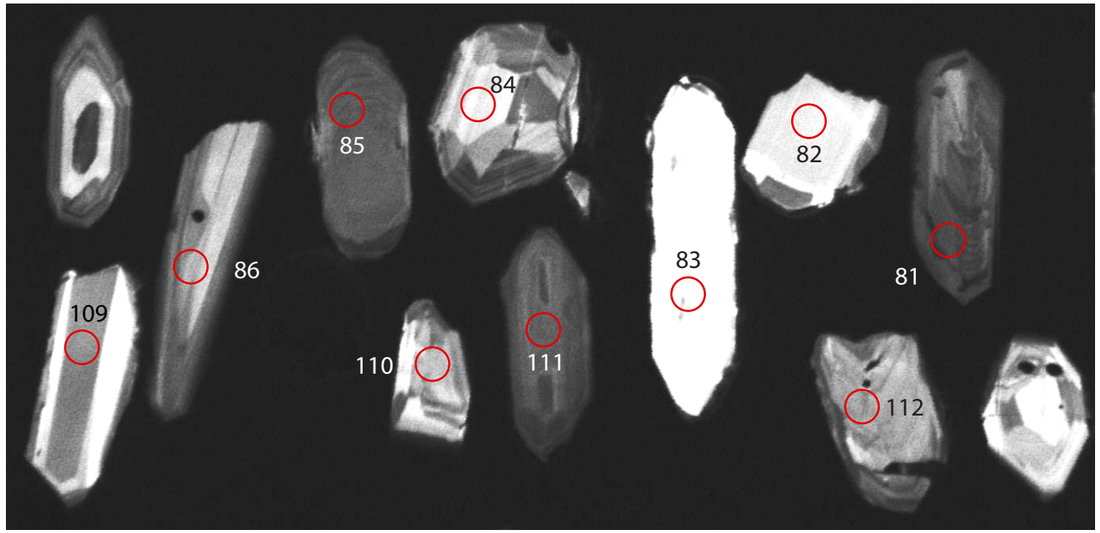

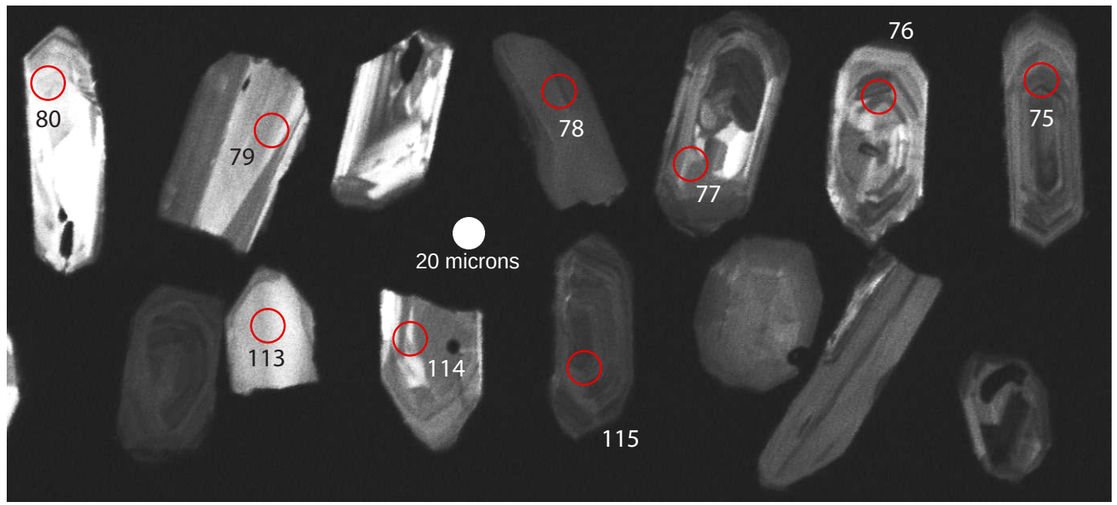

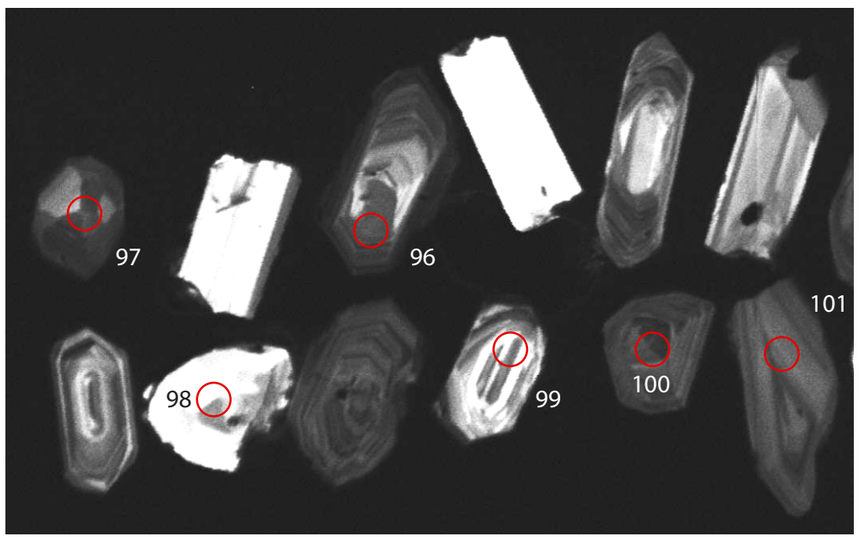

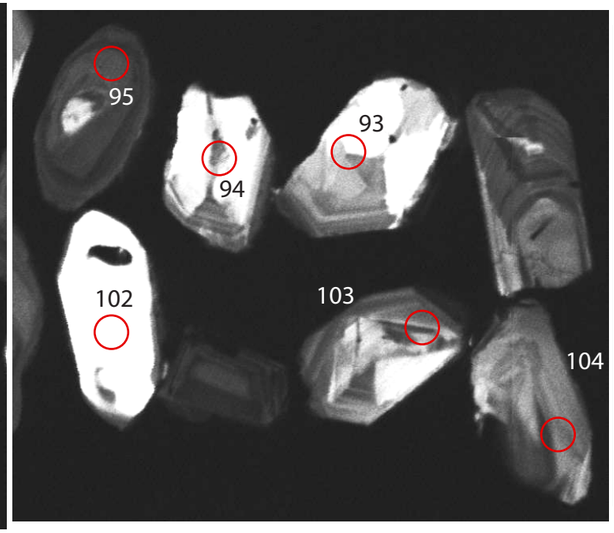

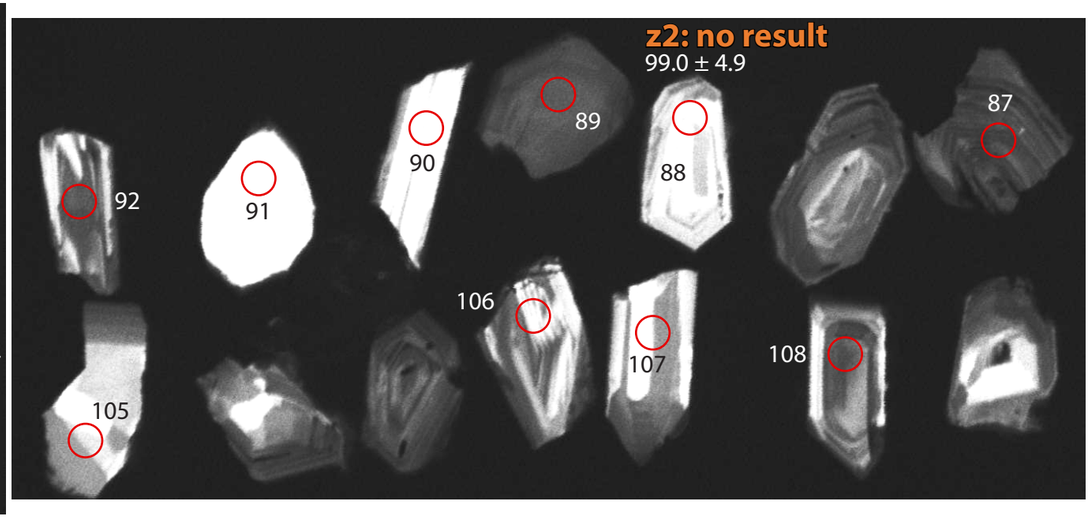

18DL002-296D M row 1 Nanushuk Formation detrital zircon AK DGGS BSU0443-0446 20Sept19

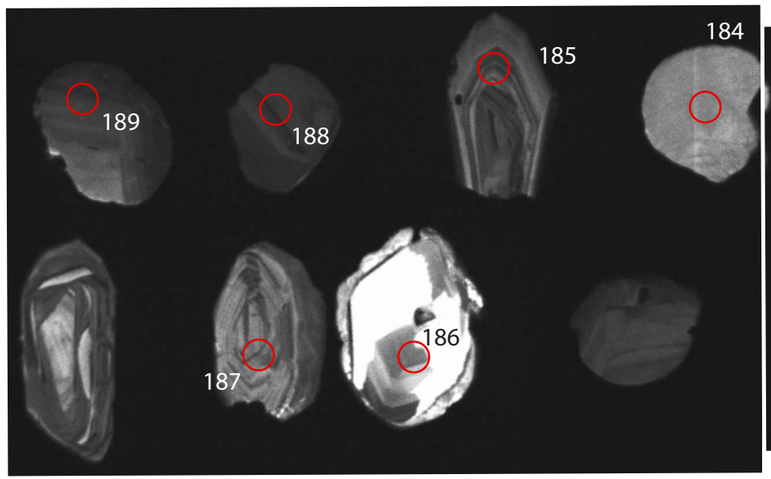

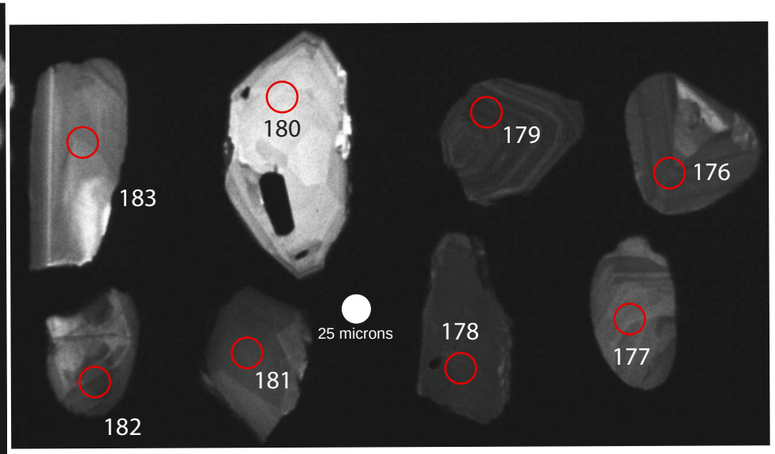

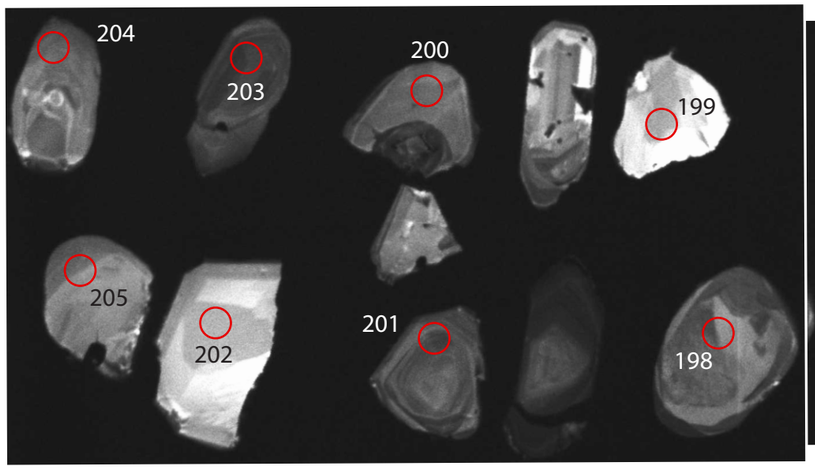

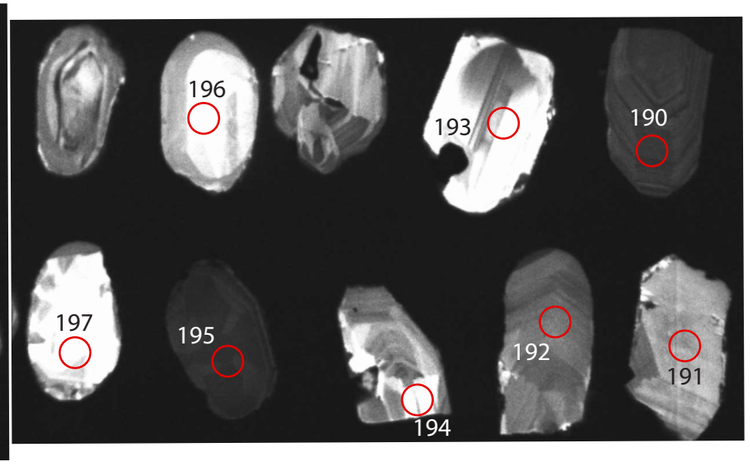

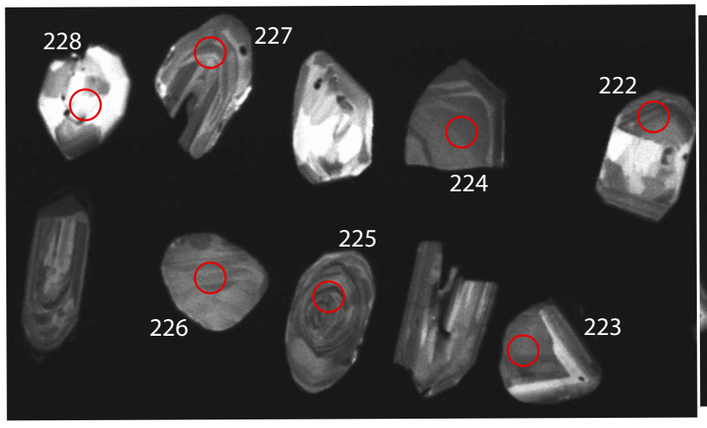

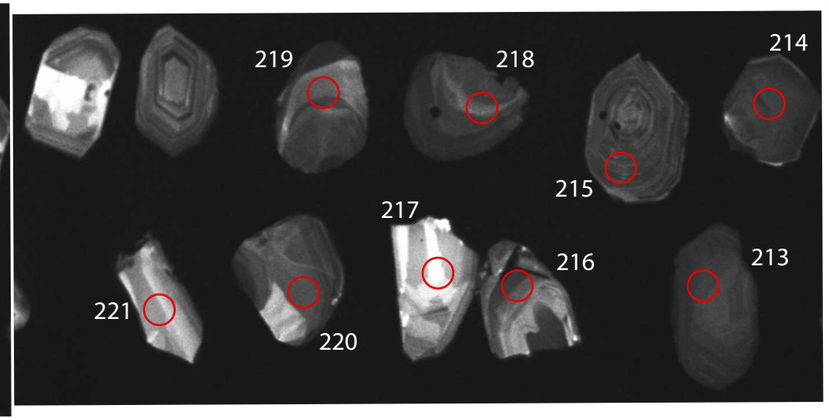

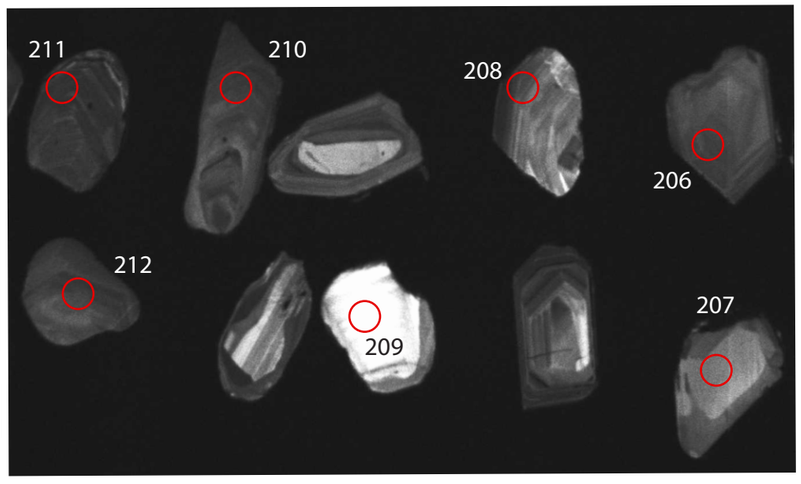

18DL002-296D M row 2 Nanushuk Formation detrital zircon AK DGGS BSU0443-0446 20Sept19

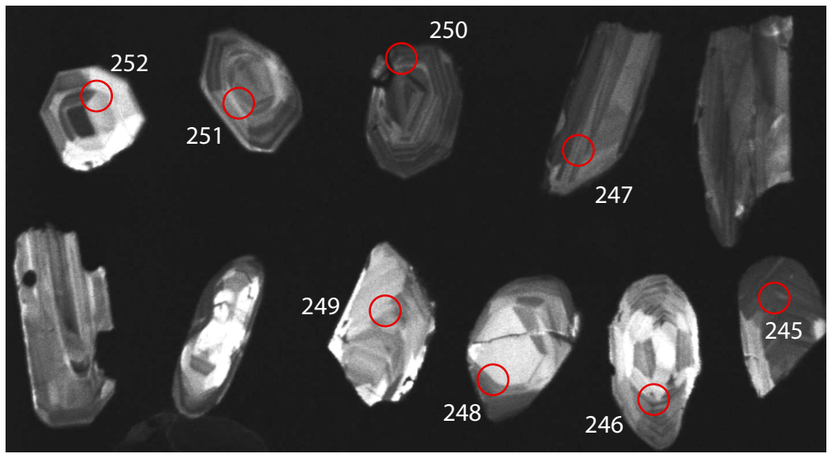

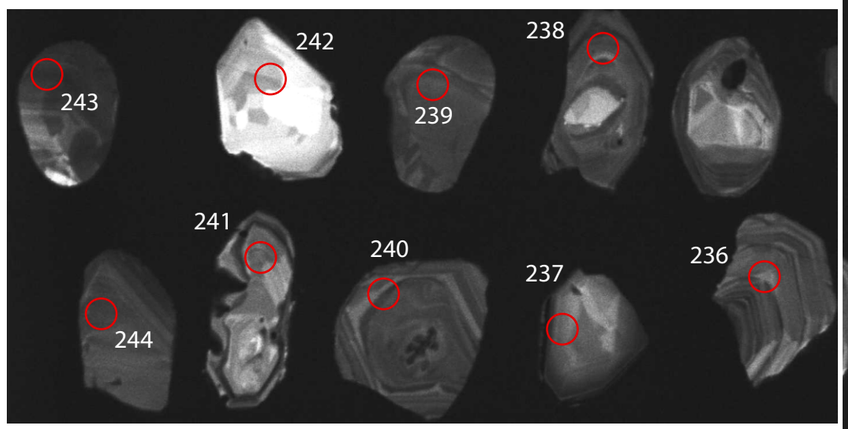

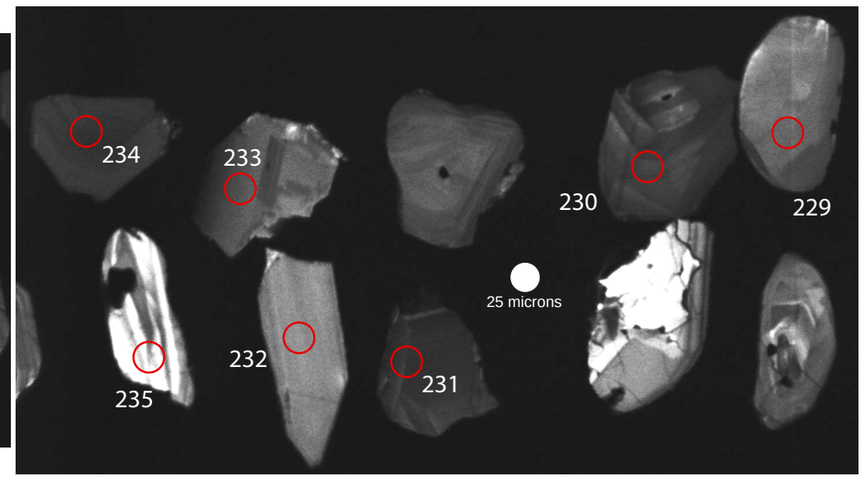

z1a: 100.90 ± 0.08
z1b: 100.78 ± 0.22

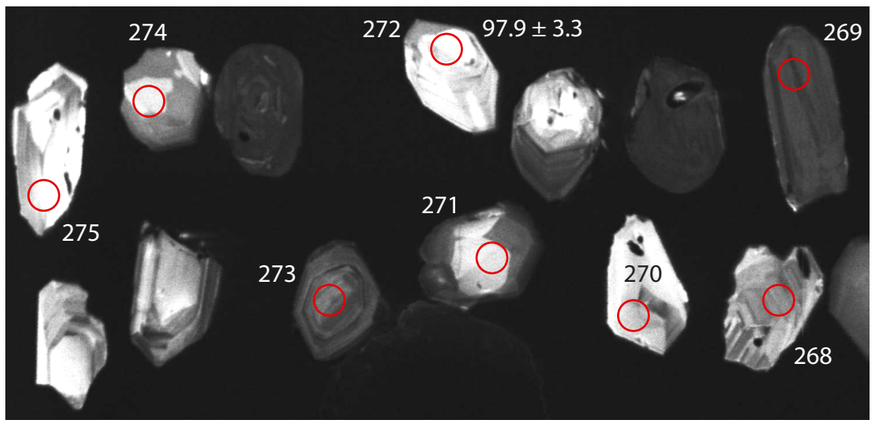

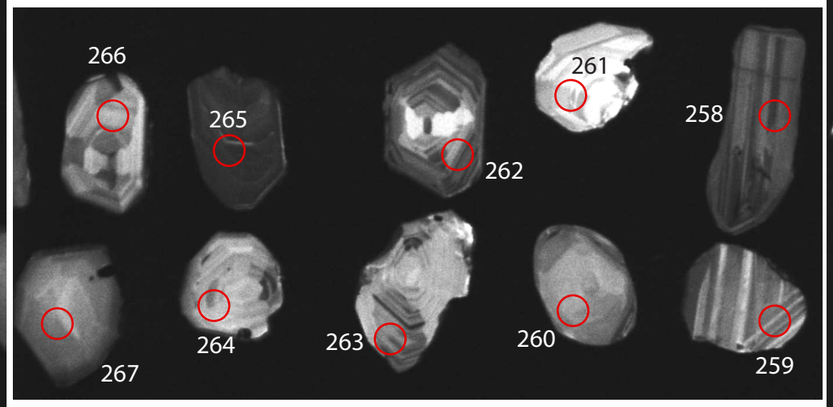

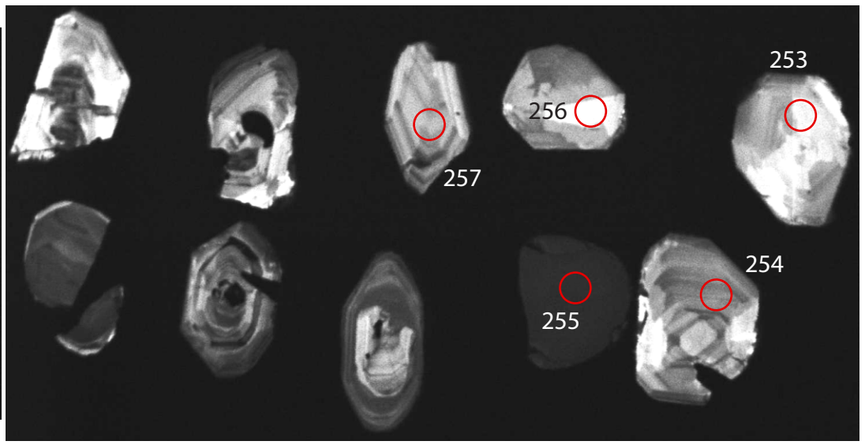

18DL002-296D M row 3 Nanushuk Formation detrital zircon AK DGGS BSU0443-0446 20Sept19

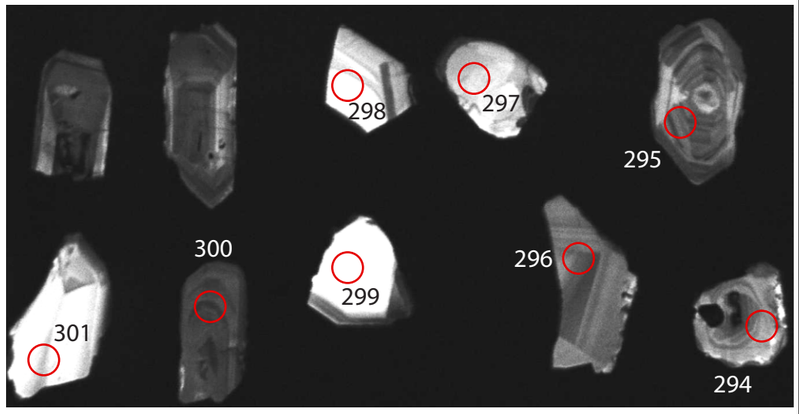

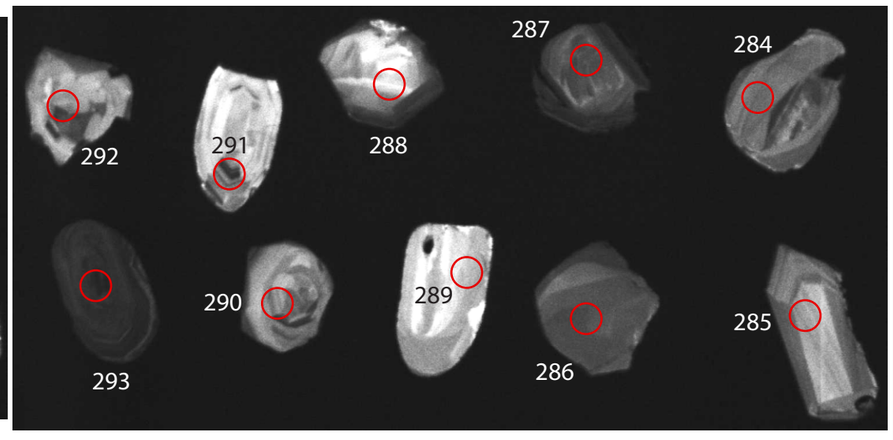

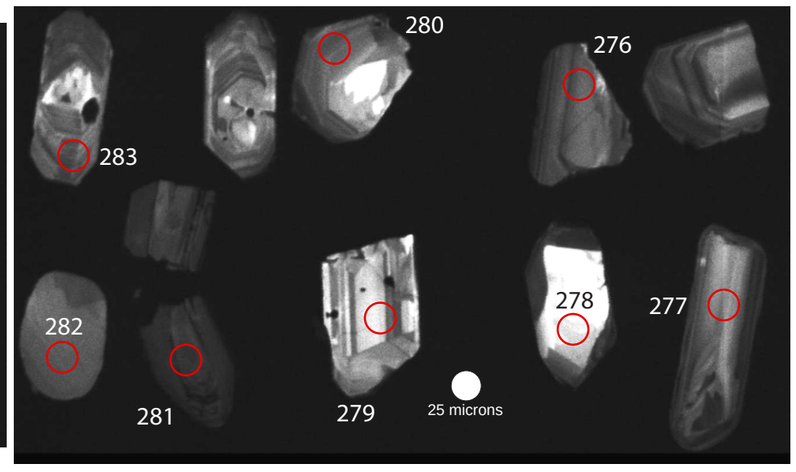

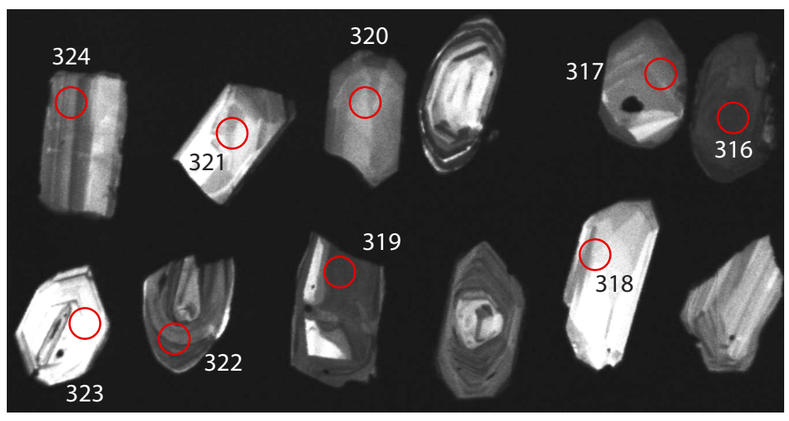

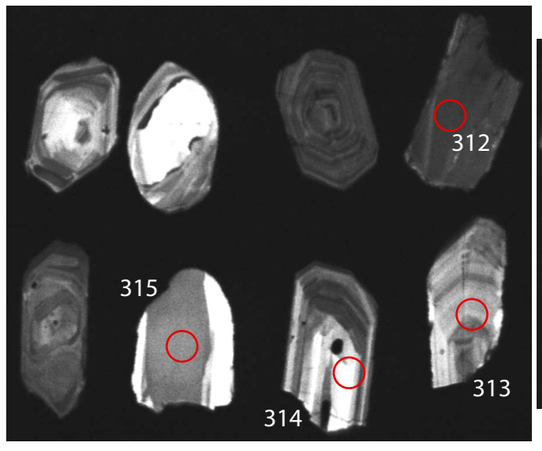

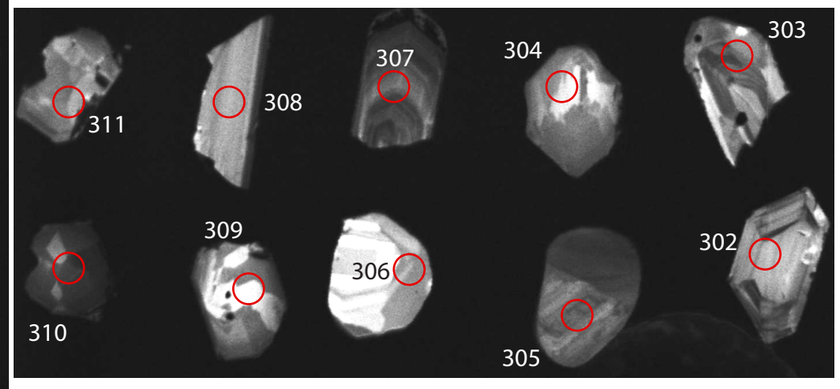

18DL002-296D S Nanushuk Formation detrital zircon AK DGGS BSU0443-0446 20Sept19

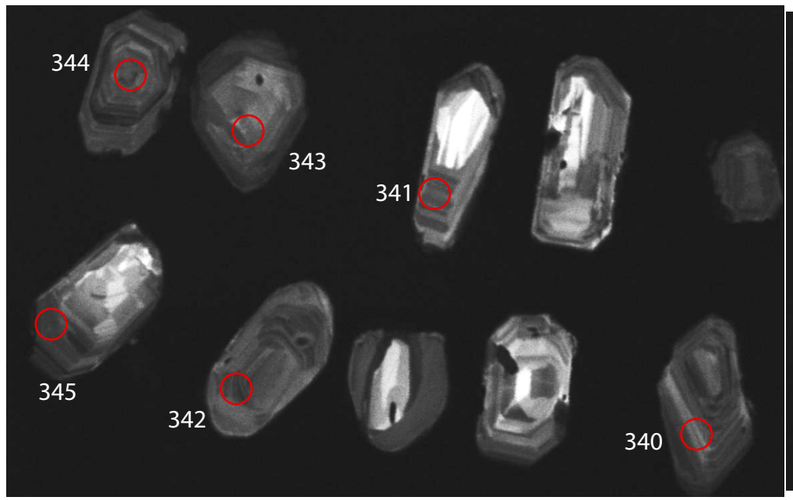

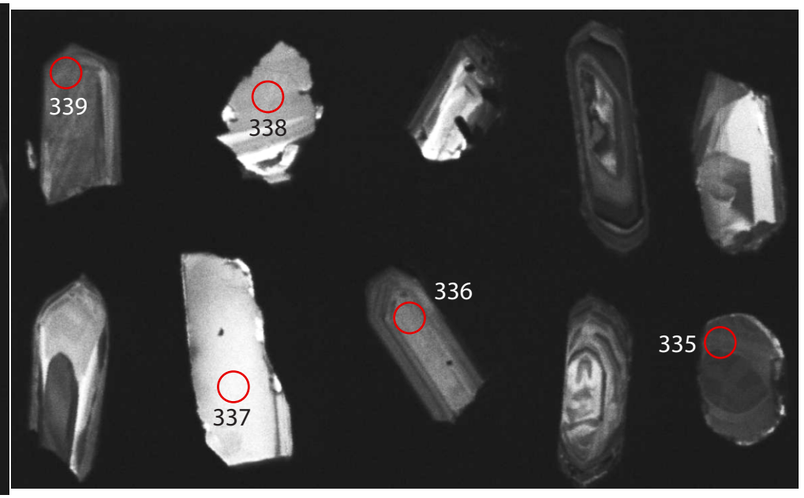

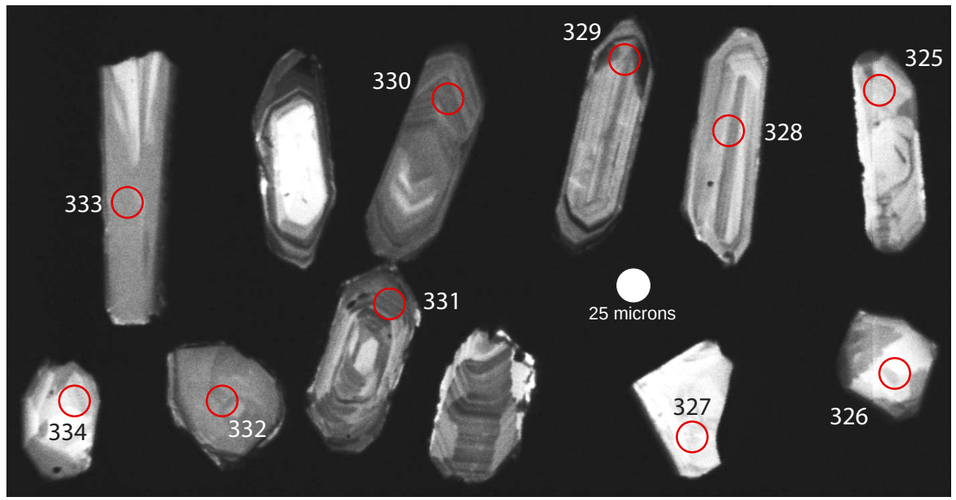

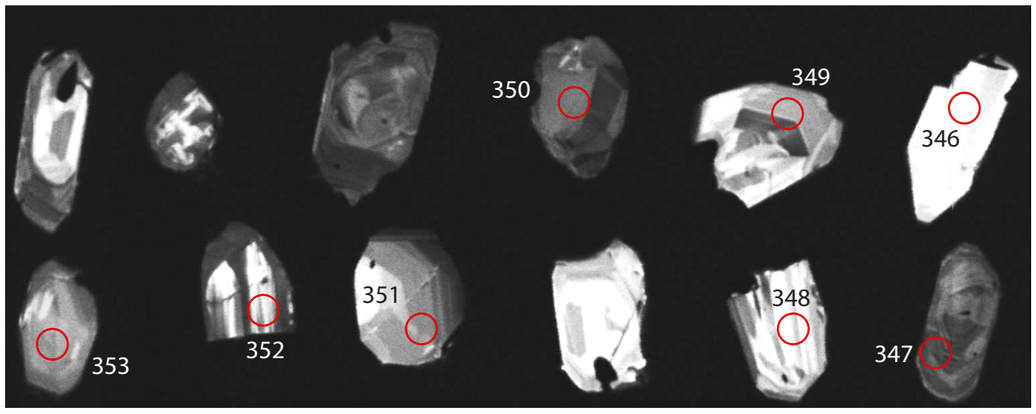

19DL011D L Nanushuk Formation detrital zircon AK DGGS BSU0659-0661, 668 18May21

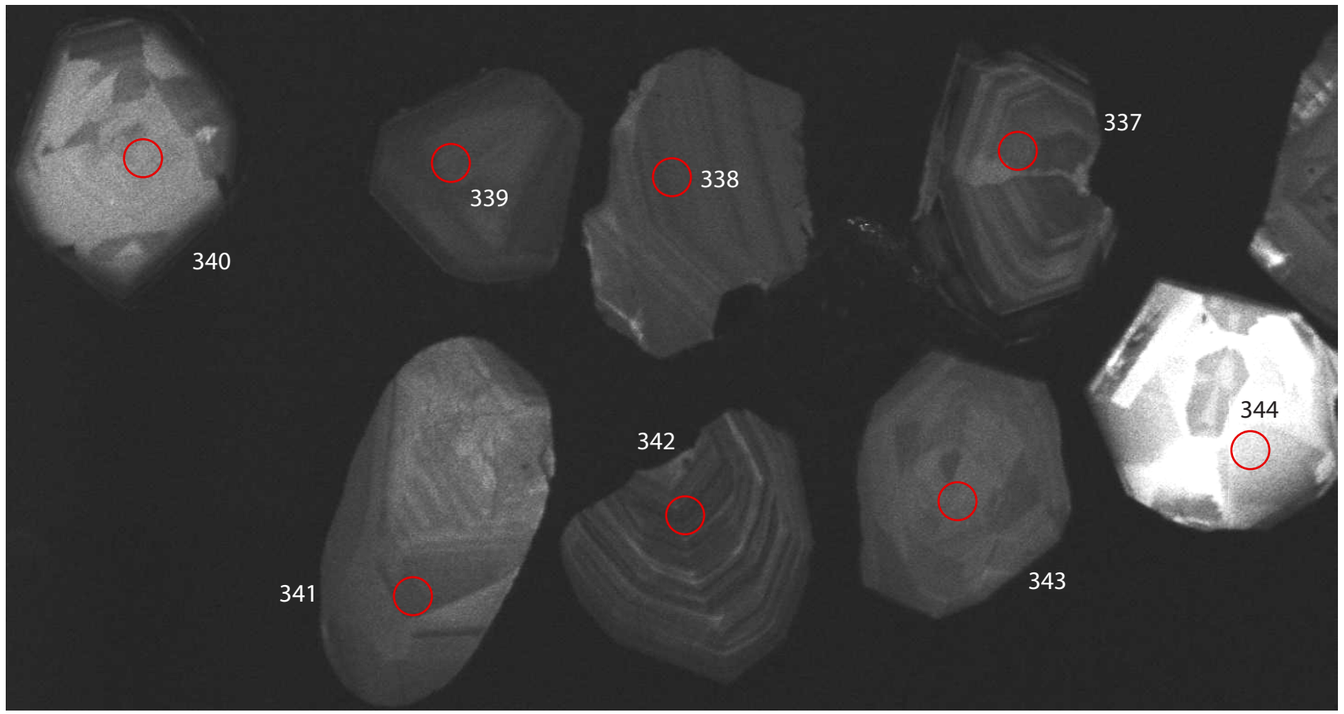

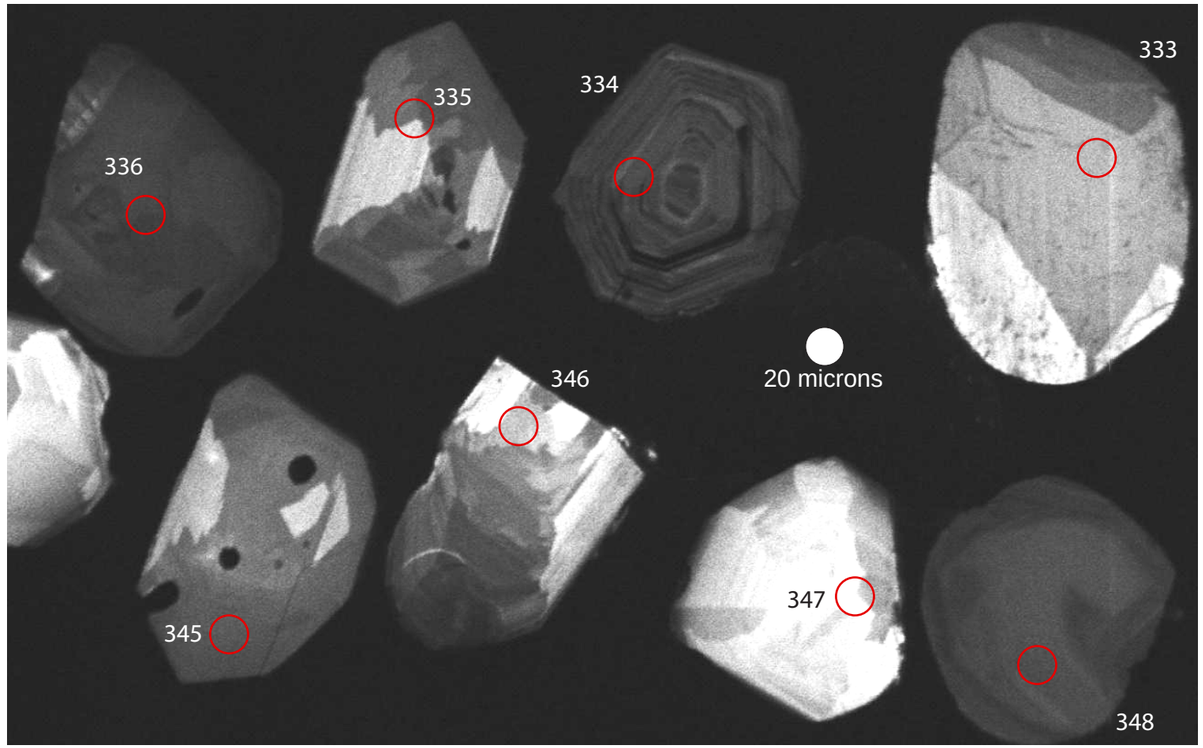

19DL011D M row 1 Nanushuk Formation detrital zircon AK DGGS BSU0659-0661, 668 18May21

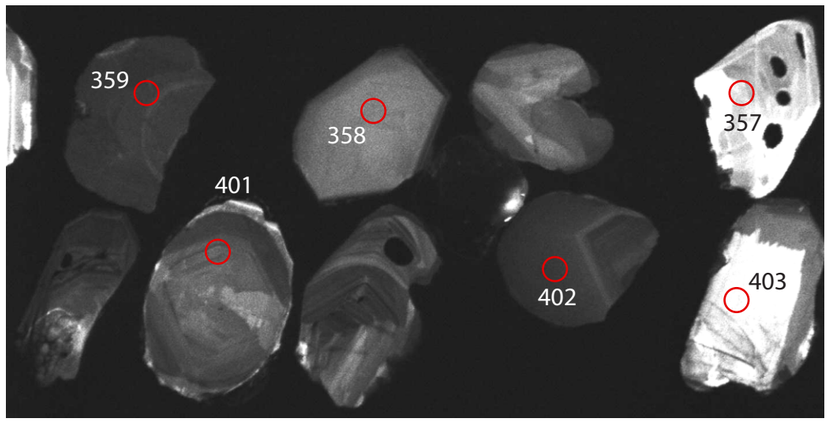

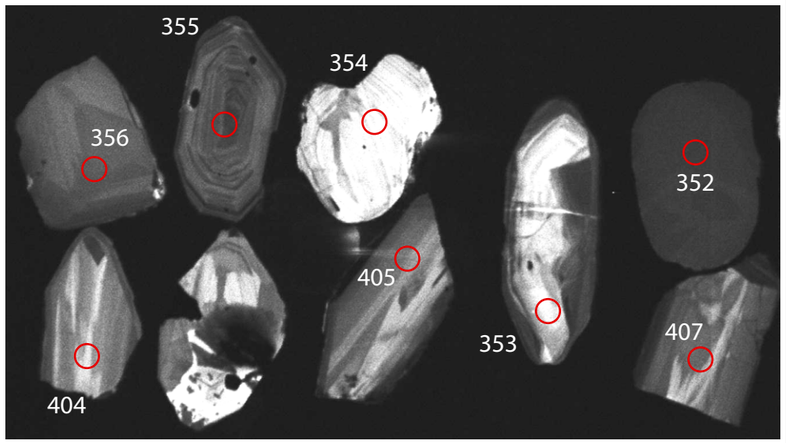

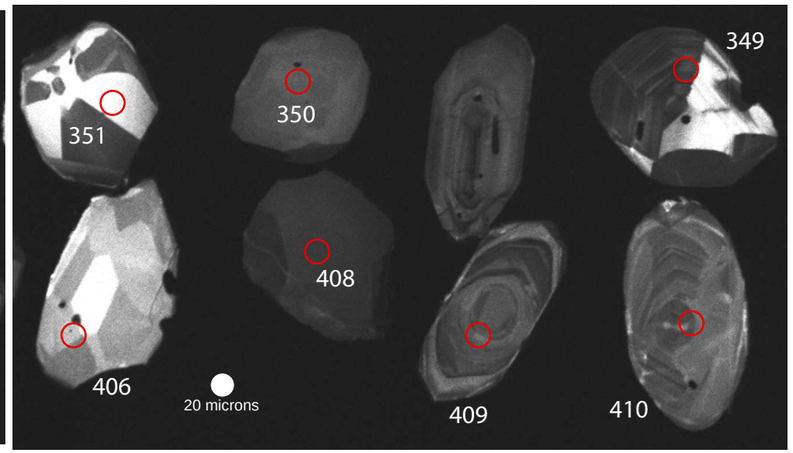

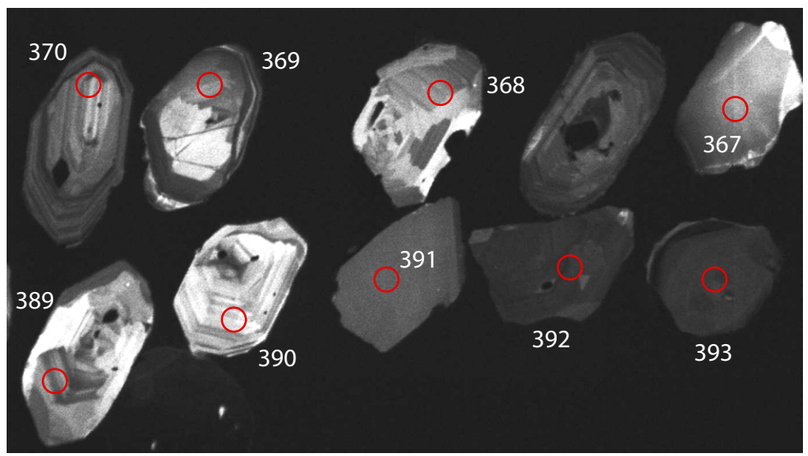

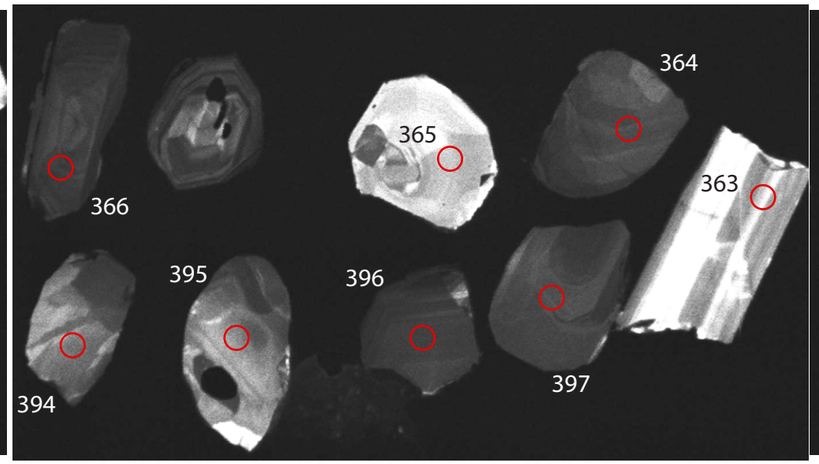

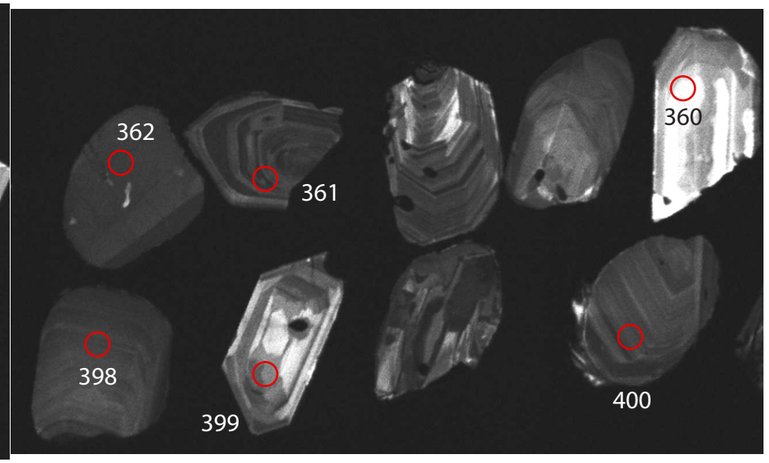

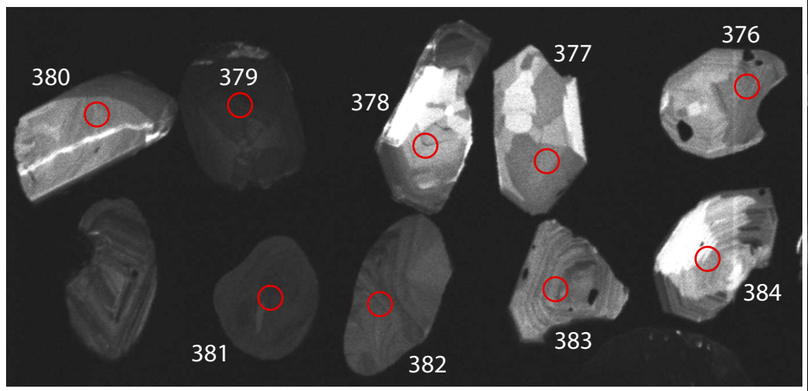

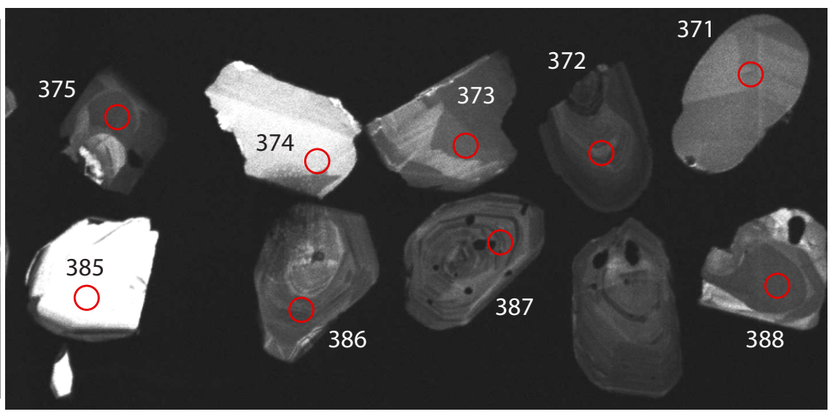

19DL011D M row 2 Nanushuk Formation detrital zircon AK DGGS BSU0659-0661, 668 18May21

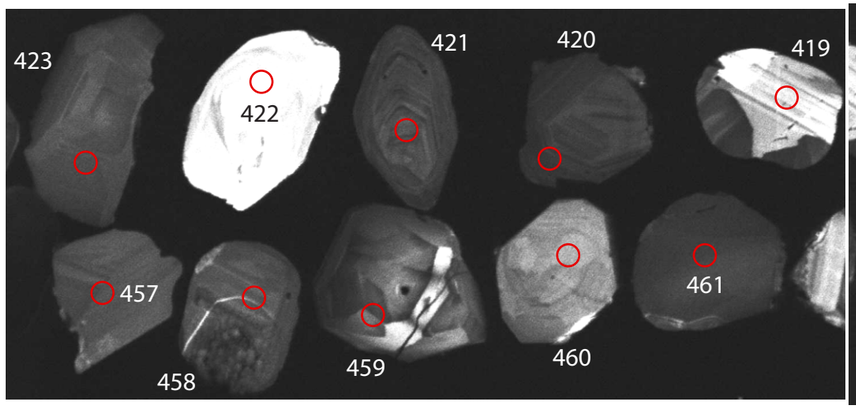

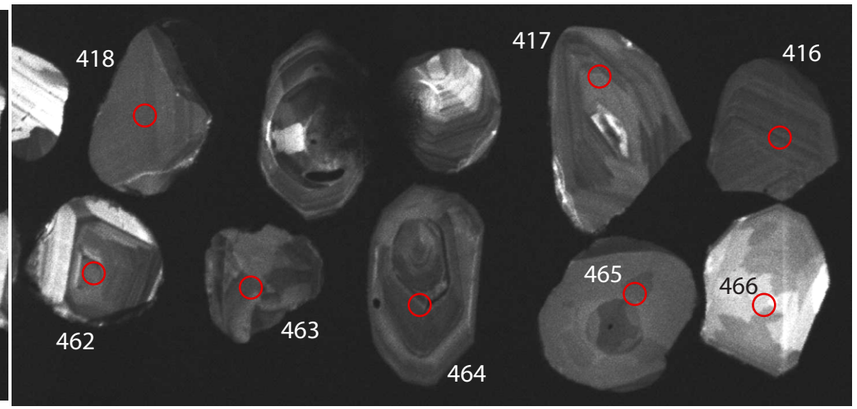

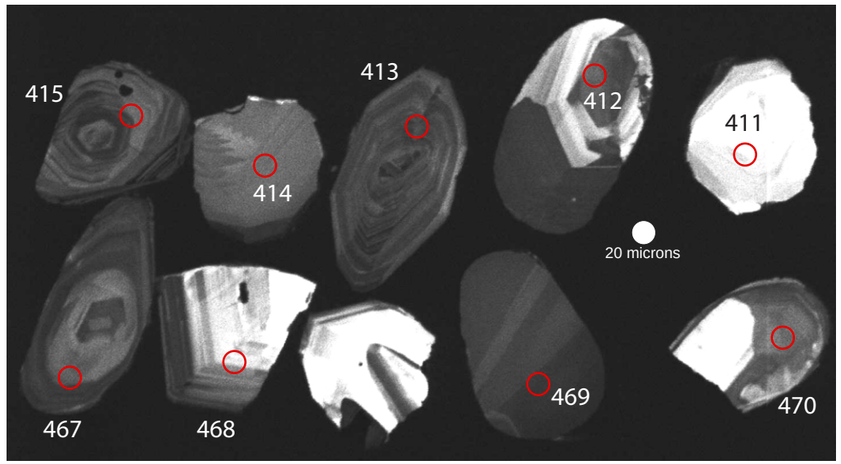

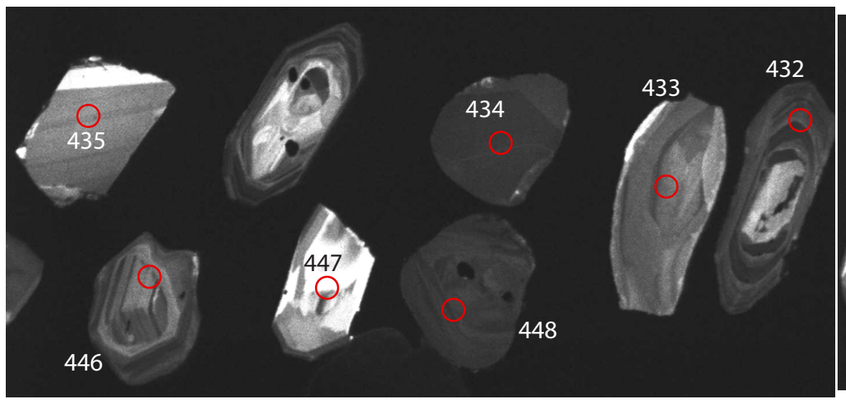

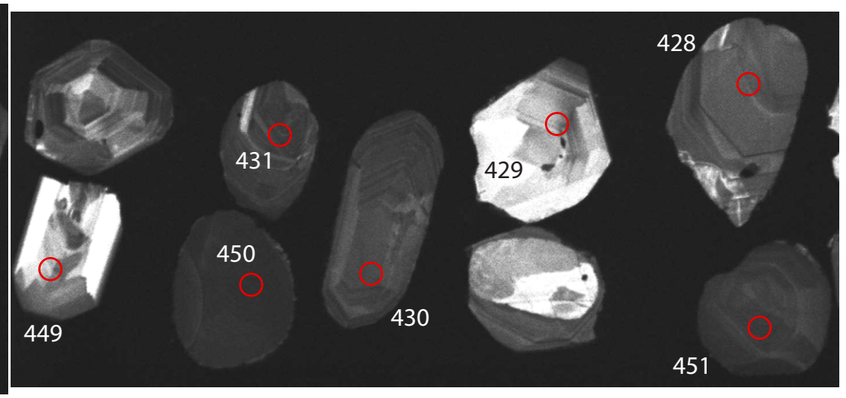

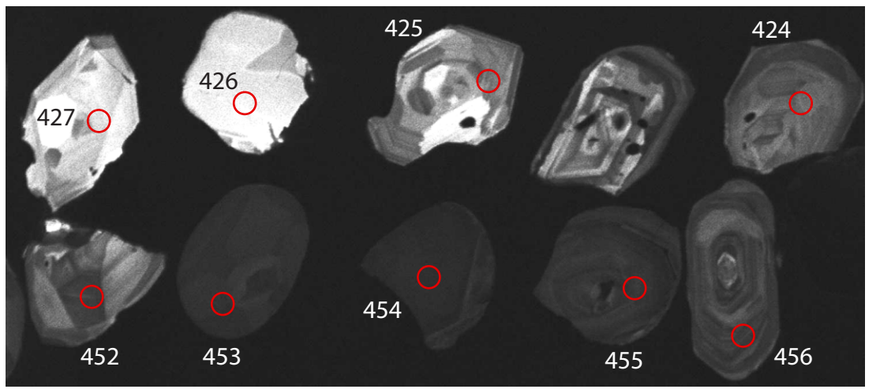

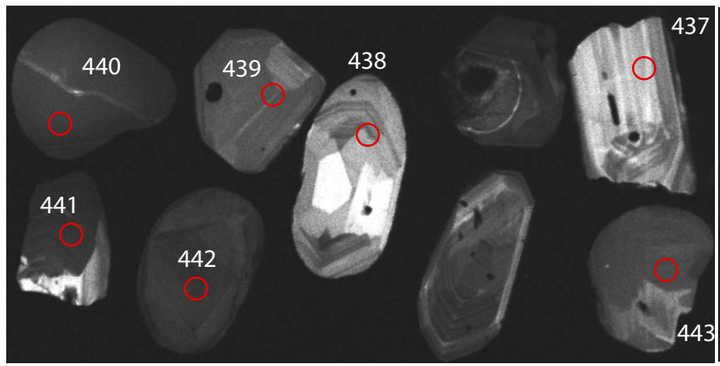

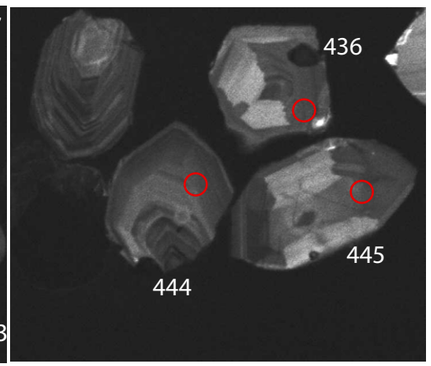

19DL011D S row 1 Nanushuk Formation detrital zircon AK DGGS BSU0659-0661, 668 18May21

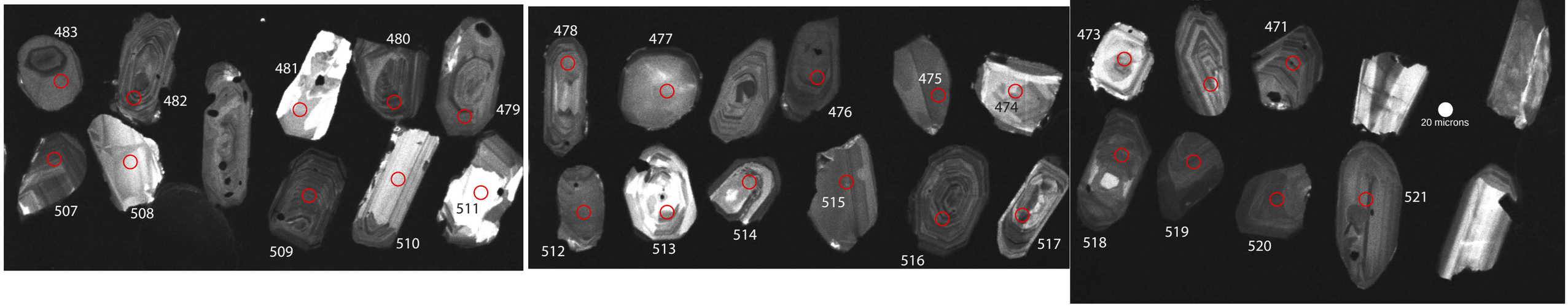

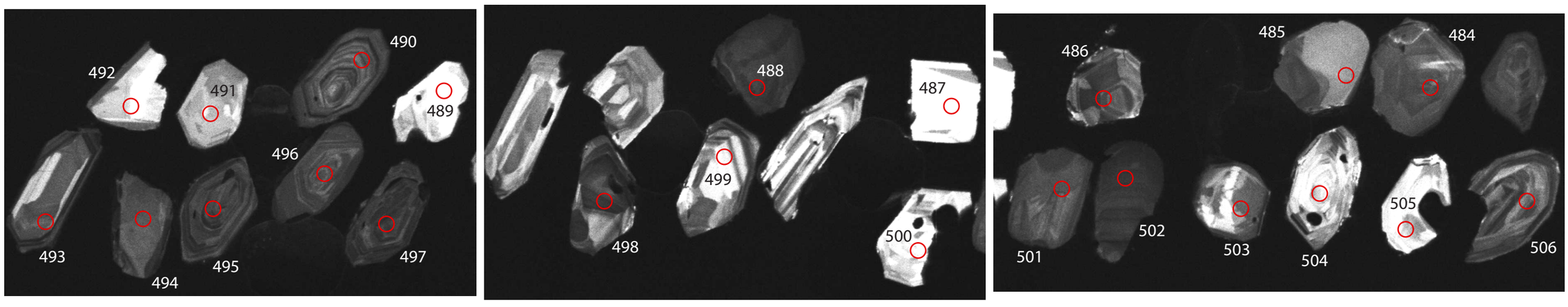

19DL011D S row 2 Nanushuk Formation detrital zircon AK DGGS BSU0659-0661, 668 18May21

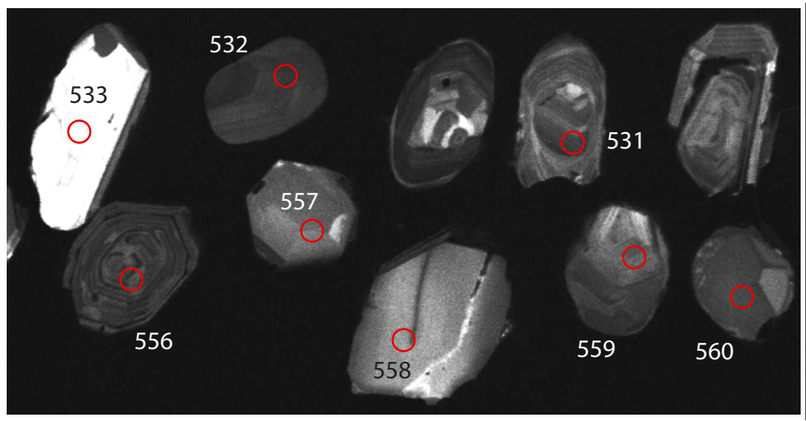

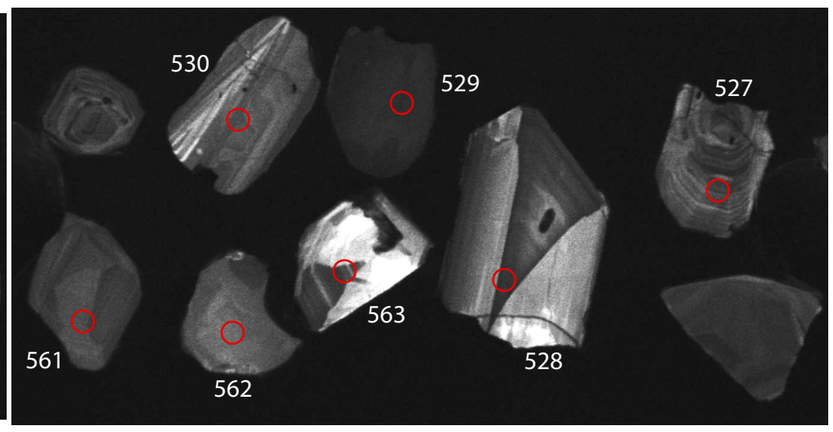

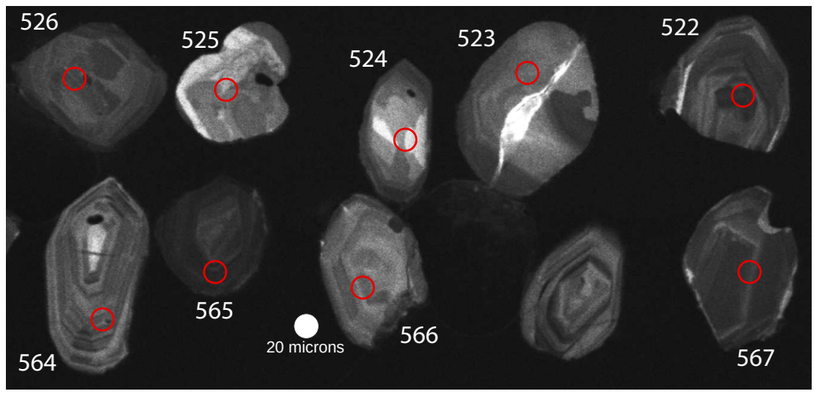

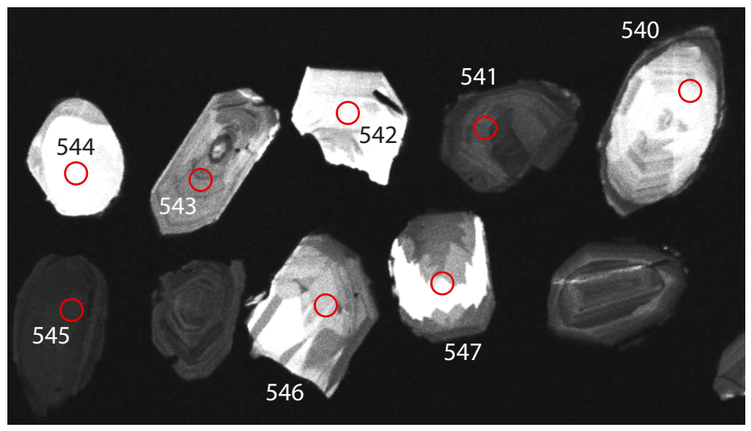

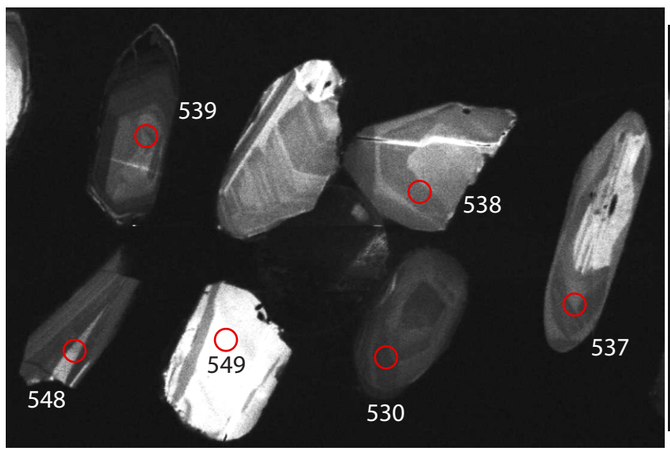

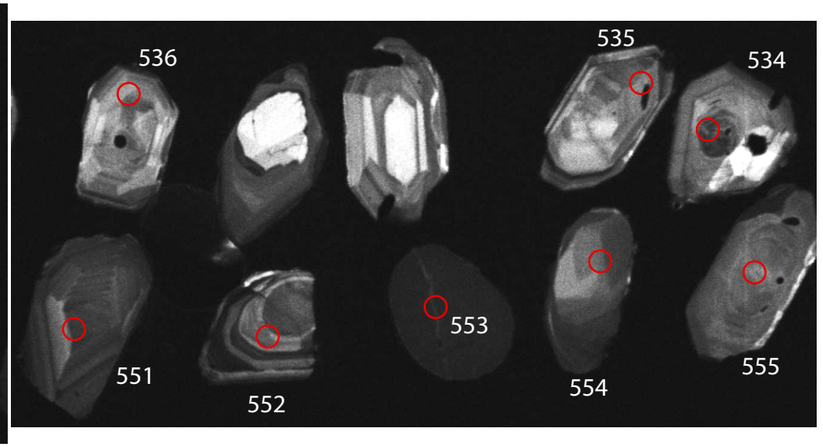

19DL010D	S	Nanushuk Formation	detrital zircon	AK DGGS	BSU0630-0634	24Feb21

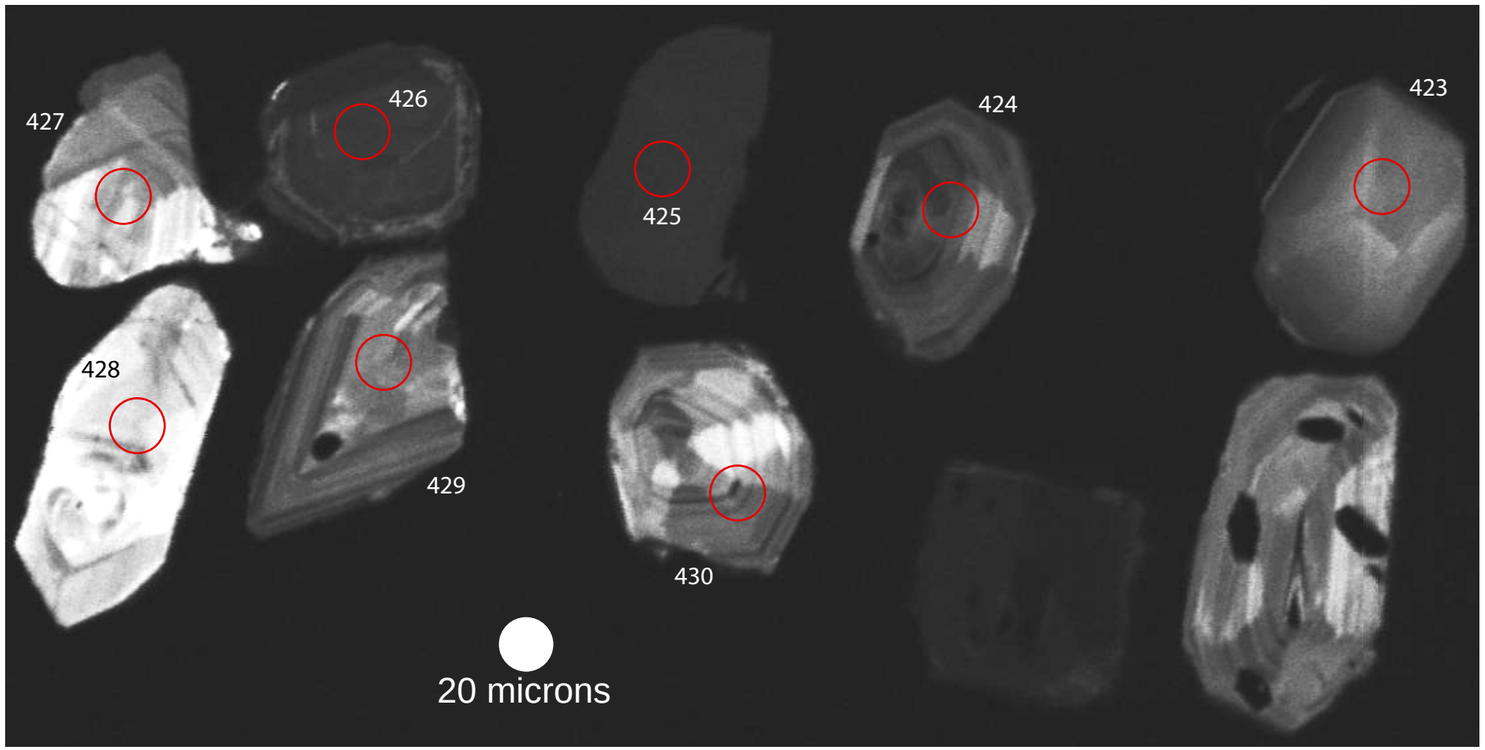

19DL010D XS row 1 Nanushuk Formation detrital zircon AK DGGS BSU0630-0634 24Feb21

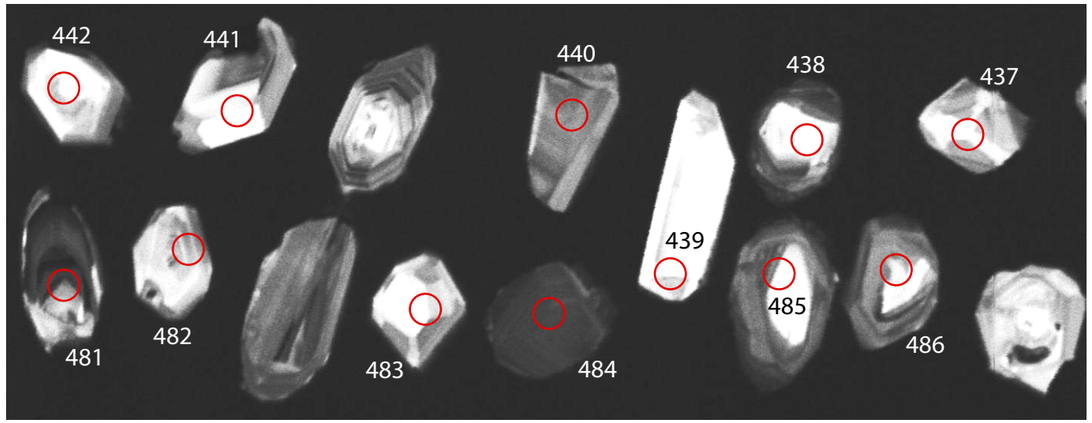

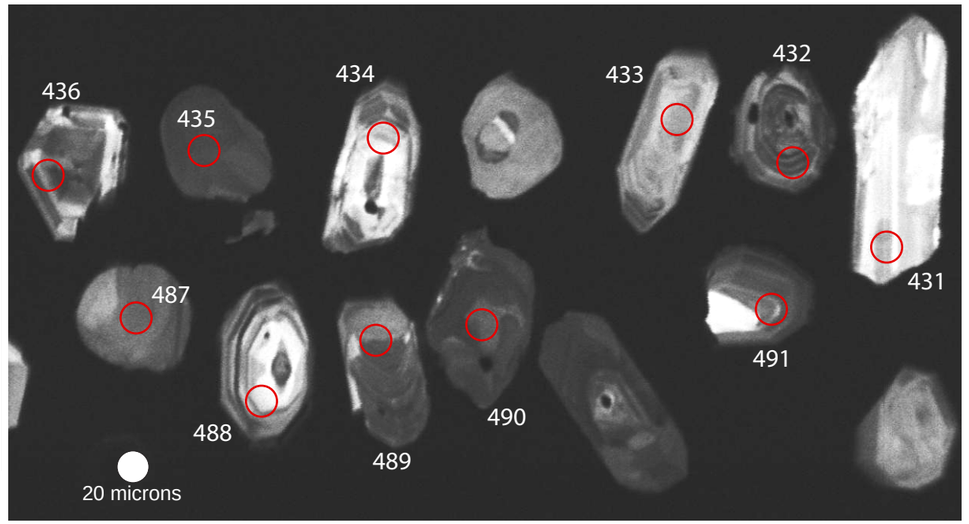

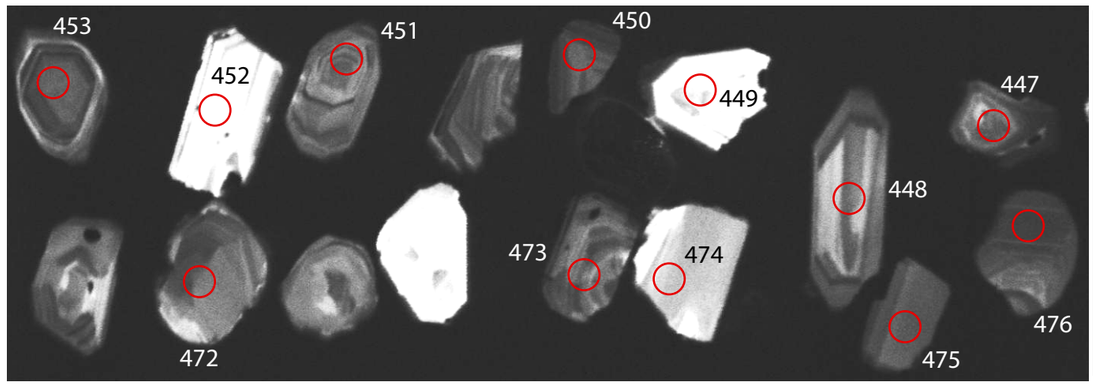

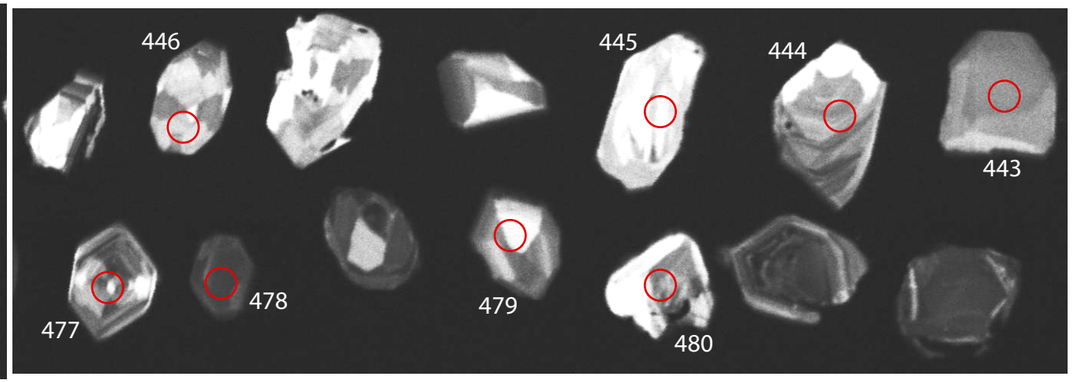

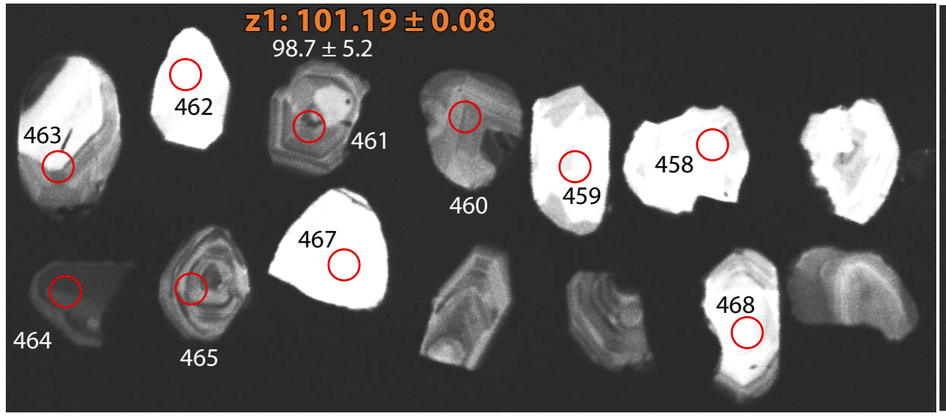

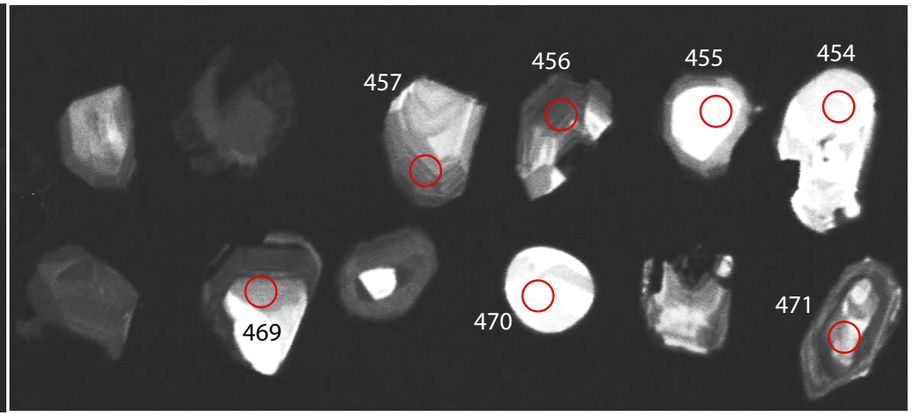

19DL010D XS row 2 Nanushuk Formation detrital zircon AK DGGS BSU0630-0634 24Feb21

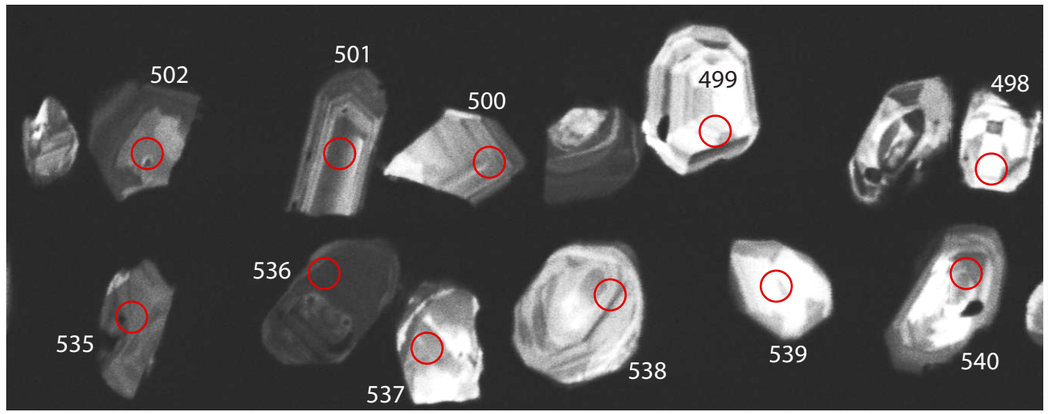

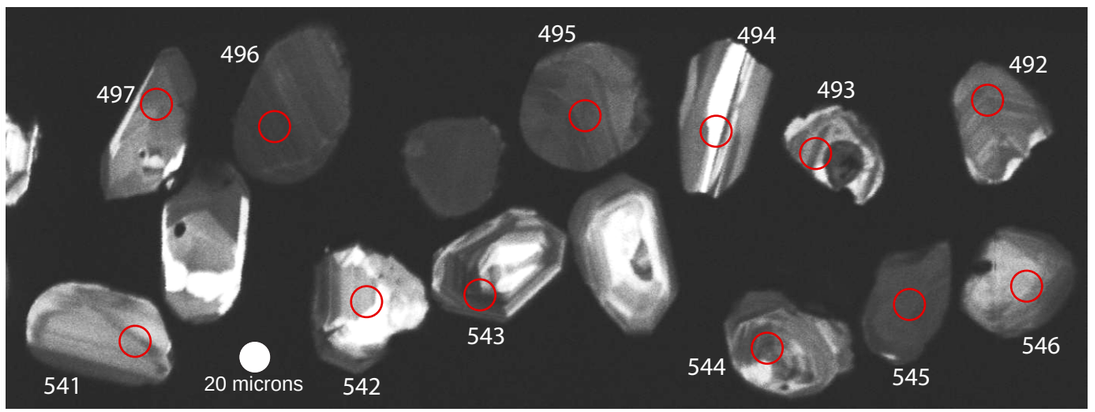

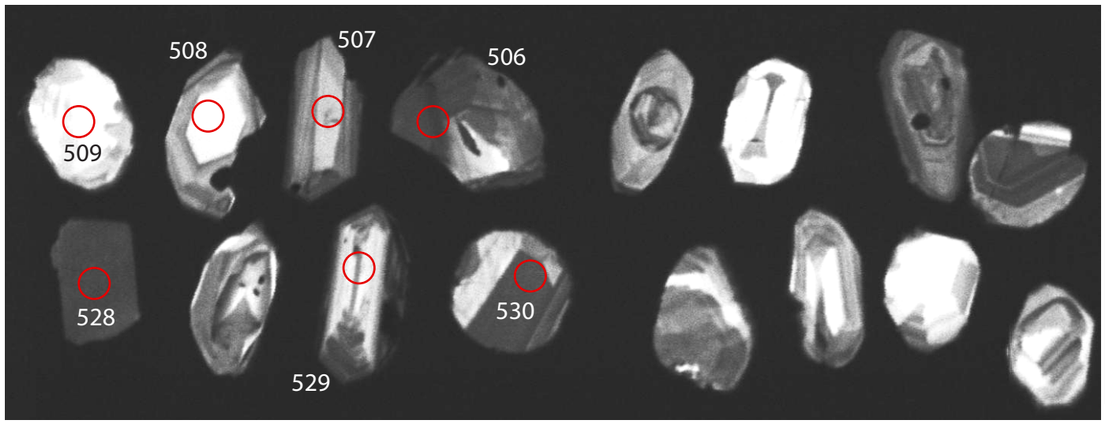

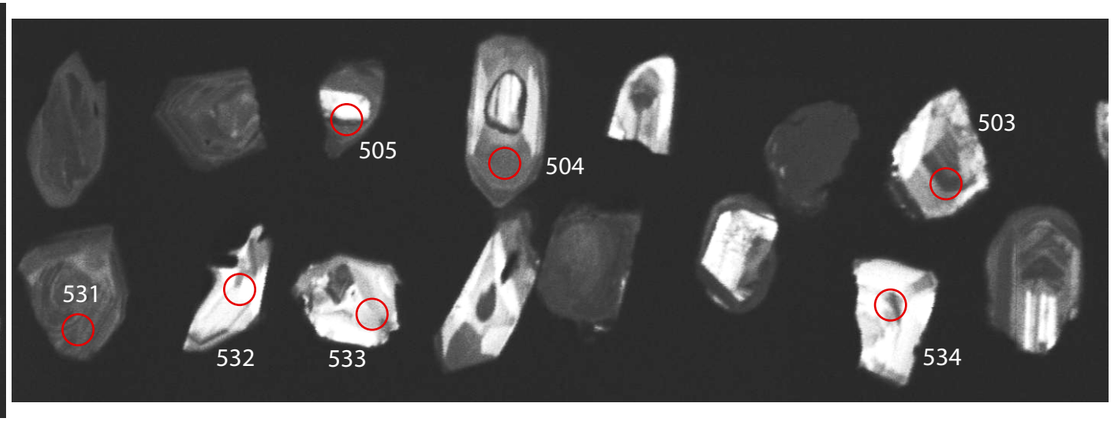

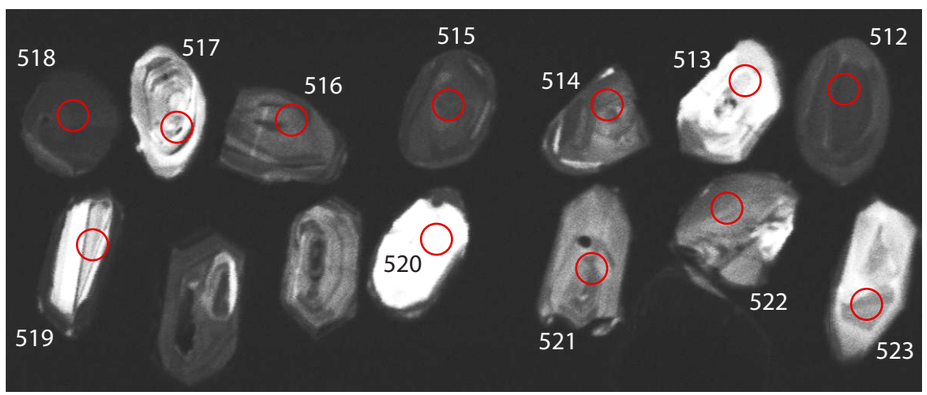

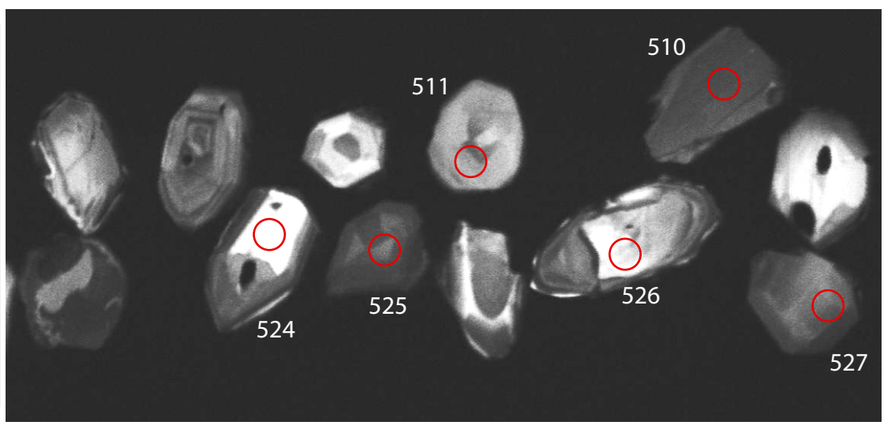

18DL002-0.8D S Torok Formation detrital zircon AK DGGS BSU0443-0446 20Sept19

Row 1

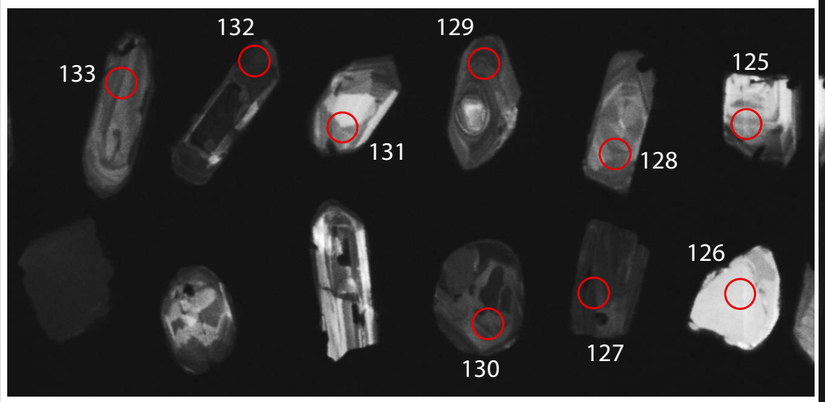

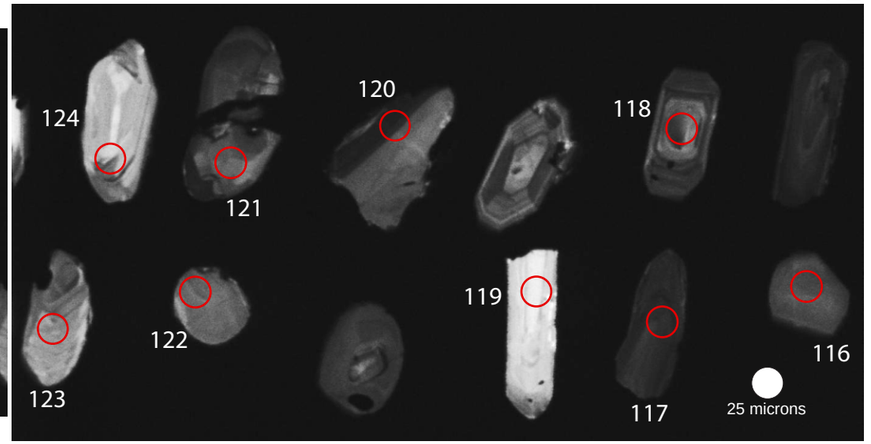

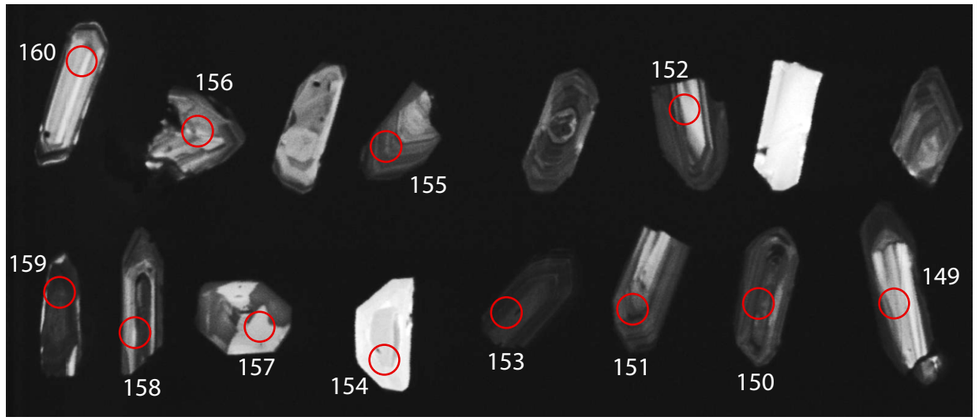

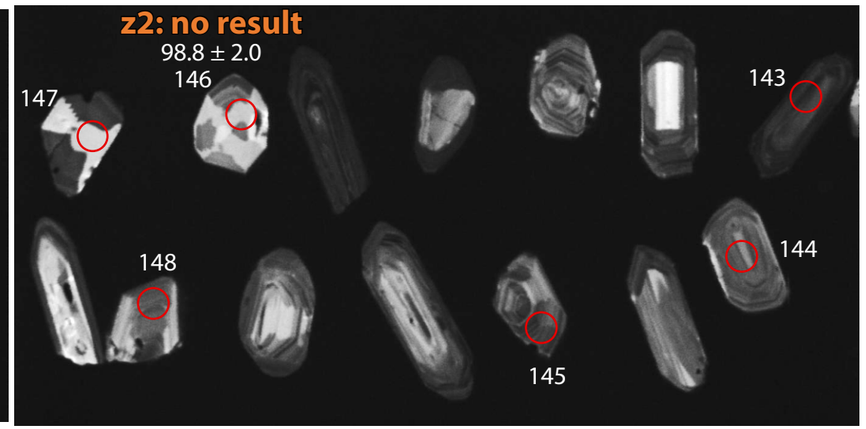

Row 2